On the Thermal Anomaly of Lake Untersee

James Bevington

August 21, 2015

International Space University MSS15

Internship Report

Abstract

Reported here is the outcome from a student internship undertaken with Dr. Chris McKay at the NASA Ames Research Center. The project for this internship focuses on Lake Untersee, an Earth analog for icy moons. The anoxic hole of Lake Untersee has a thermal bump that was first observed by Wand et al., 1997 and has been confirmed several times (Wand et al., 2006; Andersen 2011). The expected thermal profile of the hole is linear from 0C at the thermocline to ~4C, the ground temperature in Antarctica, at the bottom. Instead, there is an increase from 0C near the thermocline to 5C which is maintained for 7m, then a linear profile to ~4C near the bottom. Thermal modeling was conducted to quantify the energy input required to maintain the bump. The results revealed 2 sources. Chemical reactions and radiative energy were analyzed as possible explanation. The chemical analysis revealed a peak in Chlorophyll a at the same depth as the shallower source and several interesting reactions with maximum rates at the same location as the lower depth source. However, the energy released from these reactions was orders of magnitude smaller than required source. The radiation analysis revealed a profile with two peaks in similar locations to the sources and a total energy input within a factor of 1.5 of the required sources. The conclusion from this work is that photosynthesis and the chemical reactions support microbial life in the water column which in turn acts as an opacity to convert radiative energy into thermal energy. Recommendations for future work are aimed at quantifying the quantity and types of microbes present in the water column. Beyond the work of the project, two field trips are described and a discussion on benefits to the student of the internship is given.

Table of Contents

1. Introduction

To meet the requirements of the MSc of Space Studies a 12 week internship was undertaken at NASA Ames in Mountain View California, United States. Ames is one of several NASA campuses and is known for aeronautical research, collaboration with new space start-ups and reentry heat shielding. The advisor for the internship is Dr. Chris McKay, a world renowned astrobiologist. Dr. McKay conducts research aimed at biological analogs for other worlds, remote sensing of exoplanet atmospheres, and geological questions. One focus of Dr. McKay is Antarctic lake systems as analogs for icy moons of Jupiter and Saturn. This is the topic that the project for this internship investigates. The role at NASA is equivalent to a Research Assistant. Responsibilities include conducting analysis to answer research questions, processing data, communicating results in the form of journal articles or reports, collaborating with other interns to improve their projects and gaining their insight on my project, presenting my work orally, and proposing research questions related to the work of Dr. McKay.

The report is broken into 9 sections. Section 2 is intended to introduce the field of astrobiology. Sections 3-6 are technical analyses conducted during the internship including literature review (section 3) thermal analysis (section 4) unraveling the mechanisms of the thermal anomaly (section 5) and finally an analysis of the stability of the lake (section 6). Section 7 discusses some field work conducted during the internship period. The mandated "Benefits to the student of the internship" content is discussed in section 8 and concluding remarks and recommendations are made in the final section.

2. Motivation and Project Introduction

Until the 17th century, the geocentric model placed earth and its human inhabitants at the center of the universe. With arguments from Copernicus and Kepler, the center of the universe was moved to the sun until the mid-18th century when Wright and Kant proposed the Milky Way as the center. By the 1920s the Milky Way centered model was replaced. While the physical center has been moved away from the human centric ideology, the idea that humans are alone is currently the leading model of life in the universe. Like the paradigm shifts before it, the current era is marked by heated, philosophical debate with only circumstantial evidence and as support. To many, the discovery of other life forms in the universe is only a matter of time. But till that time, comes and direct supporting evidence exists neither model can be confirmed.

In search of evidence for life one must know what to look for. Currently, there is no single accepted definition of life. NASA proposes the following definition, "a self-sustaining chemical system capable of Darwinian evolution (Simon Fraser University, 2015)." However, many researchers relate to Potter Stewarts's statement, "I can't define it but I know it when I see it." This statement illustrates an important point. The modern understanding of life is very poor. The budding field of biological engineering can confirm this. Unlike other engineering fields, biological engineering relies on non-deterministic methods such as mutagenesis. It also suffers from reproducibility issues because mechanisms cannot be described mathematically and the variability introduced between different labs and different technicians often outweighs the variability induced by the experiment. This is in grave

contrast to mechanical engineering for example which is based largely on classical physics which are well understood and often derived from first principals.

One reason that current understanding of life is poor is because all current models are derived from one tree of life, the one found on earth. Anyone who has traveled abroad or learned a second language will tell you that the experience of a second model strengthens understanding of the original model. This argument can be extended to science. It would be very difficult to unravel the mechanisms of chemical bonding from only one molecule. Likewise, unraveling the mysteries of life and developing a deep comprehension is hindered by access to only one tree of life. A second tree of life would provide opportunity to compare and contrast observations made on earth's tree leading to a more solid understanding.

But, where can one expect to find a second example of life? The current search for extraterrestrial life is limited by practicality and physical constraints. As no human spacecraft has traveled to another star, the search with physical implementations is limited to the solar system for the foreseeable future. And while different life forms can be conceived, the most obvious constraints to narrow the search would be to look for things that resemble earth life prior to expanding the search (McKay personal communication). Thus, the two major constraints would be to focus on carbon based life and the requirement for liquid water which are the primary commonalities between all earth organisms (McKay personal communication). With this in mind, two environments immediately arise to the top of the candidate list for finding life in the solar system. The first is Mars and the second are icy moons of Jupiter and Saturn.

Mars in known to have frozen water at its poles, liquid water below the surface, and was potential dominated by water features in its past. Moreover, organic carbon-based molecules have been observed on Mars. Icy moons like Europa and Enceladus also have been confirmed to have water and organic molecules. These three sites are an excellent place to look for life.

The current approach to probing other worlds thus far has been limited to remote sensing and occasionally a lander of some sort. Of the three top candidates, Mars is by far the most explored with about 11 orbiters, 6 successful landers, and 3 rovers (Tate, 2013) as summarized in figure 1. But to date a sample has not been returned to earth even from Mars. Thus, the tools for probing are limited and the opportunities to probe are even more limited. So unlike the standard suit of assays and protocols used to detect life on earth environments, the types of measurements that can be made on other worlds are limited. But, within this limited framework, it is critical to be able to positively identify life. To alleviate the issue, it helps to broaden the scope of the search. Thus instead of trying to detect life directly, searching for indications of life can be more practical. The signs are often referred to as biomarkers.

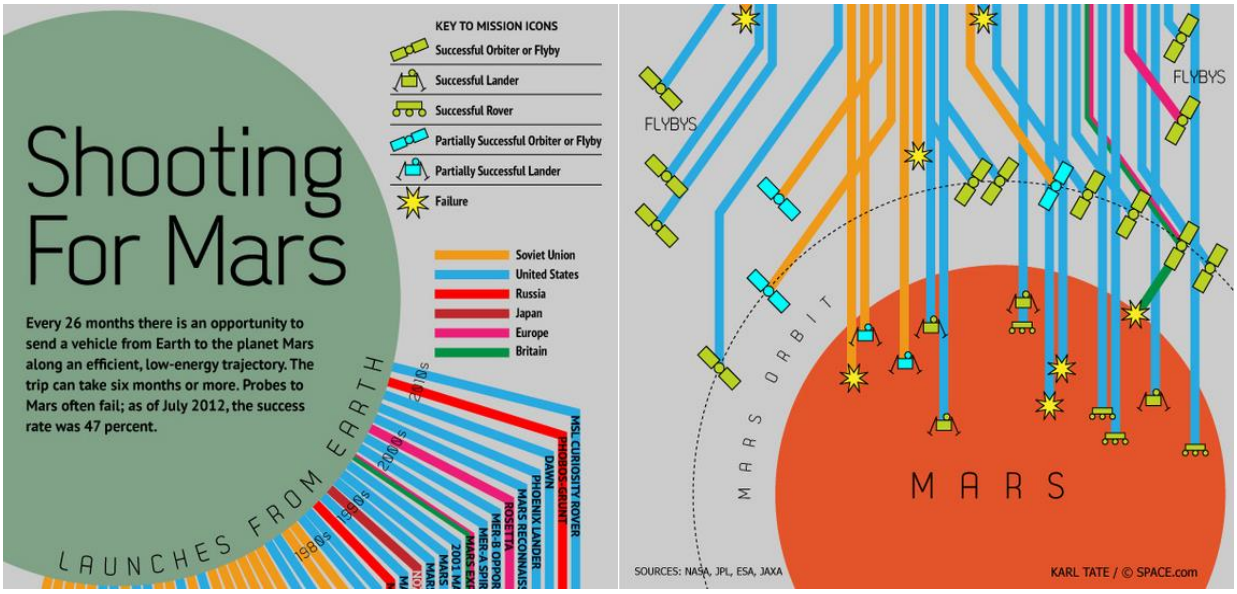

Figure 1. Summary of Mars exploration including orbiters, landers, and orbiters. Since the making of this infographic, ISRO's Mars Orbiter Mission and NASA's Maven have been successfully inserted into orbit around Mars. Image credit: Tate

Biomarkers are well defined signals that arise as a result of a living system. One of the best known biomarkers is the preference of life to metabolize lighter isotopes over heavier ones. Knowing this, a measure of isotopic ratios can serve as a strong piece of evidence in the determination of presence or absence of life. But this is just one example. There are many biomarkers some of which may be much easier to detect as life has the capability to impact global chemical and climate cycles.

Biomarkers are developed on earth based life and ecosystems. Despite the differences between earth and other worlds like Mars, there are some environments which can be studied as analogs. The goal in studying analogs is not to directly translate findings made on earth to other worlds but to learn the mechanisms of life adapted to similar environments. Once the mechanisms are well understood, they can be extrapolated and manipulated in a more meaningful way.

One useful and popular earth analog for both Mars and some icy moons is Antarctica. In particular, the Dry Valleys is one of the driest deserts and the temperatures are among the coldest on earth. Glaciers in the Dry Valleys are the only example on earth of cold based glaciers, a form of glacier found on Mars. Antarctica also has hundreds of ice covered lakes. The diversity of these lakes in immense and conditions run from fresh to hypersaline, acidic to basic, and all are 4C or below. These lake systems can be used to study mechanisms which may act in the ice covered oceans of Enceladus and Europa.

3. Lake Untersee

Lake Untersee is an Antarctic lake located in East Antarctica. It is situated in the Otto-von-Gruber-Gebirge Mountains of central Dronning Maud Land at an elevation of 563 m above sea level. It is the largest surface lake in East Antarctica having a surface area of 11.4 Km2. The lake is largely treated in

two distinct sections similar to Lake Bonny in the Dry Valleys. The large basin is 160m deep and the small basin is 100m deep. The two basins are separated by a ridge in the floor rising to 50m of depth. Currents in the lake are temperature and density driven as the lake is covered by ice. Figure 2 illustrates the topography of the lake floor. There are two glacier faces which bound the lake acting as vertical walls. The location of these glaciers is also seen in figure 2. These glaciers create density gradients in the water column because they pull the local temperatures to 0C. At depth, the water temperature approaches 4C, the ground temperature in Antarctica. The 0C water is less dense than the 4C water causing it to rise along the glacier face resulting in mixing currents. The largest glacier face, Anuchin Glacier, lies in the large basin with a cross sectional area of 0.68km2 (Steel et al., 2015). There is a smaller glacier face that remains unnamed and boarders the smaller basin. However, its contribution to mixing is only about 1% of that of Anuchin Glacier (Steel et al., 2015). Thus, currents extend to the upper water column of the smaller basin but much not below the ridge at 50 m. Figure 3 illustrates currents in the Lake Untersee modeled from thermal driven density gradients. The lack of currents and mixing in the water column from 50 to 100m in the smaller basin permits a stagnant anoxic zone to persist.

Modeling of the anoxic basin currents and thermal fluxes has revealed a major discrepancy. The temperature profile is expected to be one of two cases. The first, pictured in figure 4, is a case where temperature is determined largely by current mixing resulting in a large change from 0C to 4C in the slightly mixed portion of the column from 50 to 65m followed by a constant 4C to the bottom. The second case accounts for diffusive heat diffusion resulting in a linear profile from 0C to 4C between 65m and the bottom and the water column above is a constant 0C. However, the measured profile deviates from both of these cases in that there is a bump in the profile between 65 and 95m. The bump was first observed by Wand et al. 1997 and has been confirmed several times since then (Wand et al., 2006; Andersen et al, 2011; McKay, personal communication, 2015). The repeatability of these measurements over an almost 20 year period demonstrates not only the existence of the bump but its stability through time. The negligible effects from peanut butter may also provide an opportunity for this stability (August et al., 1999). To explain this bump, an input of thermal energy is needed.

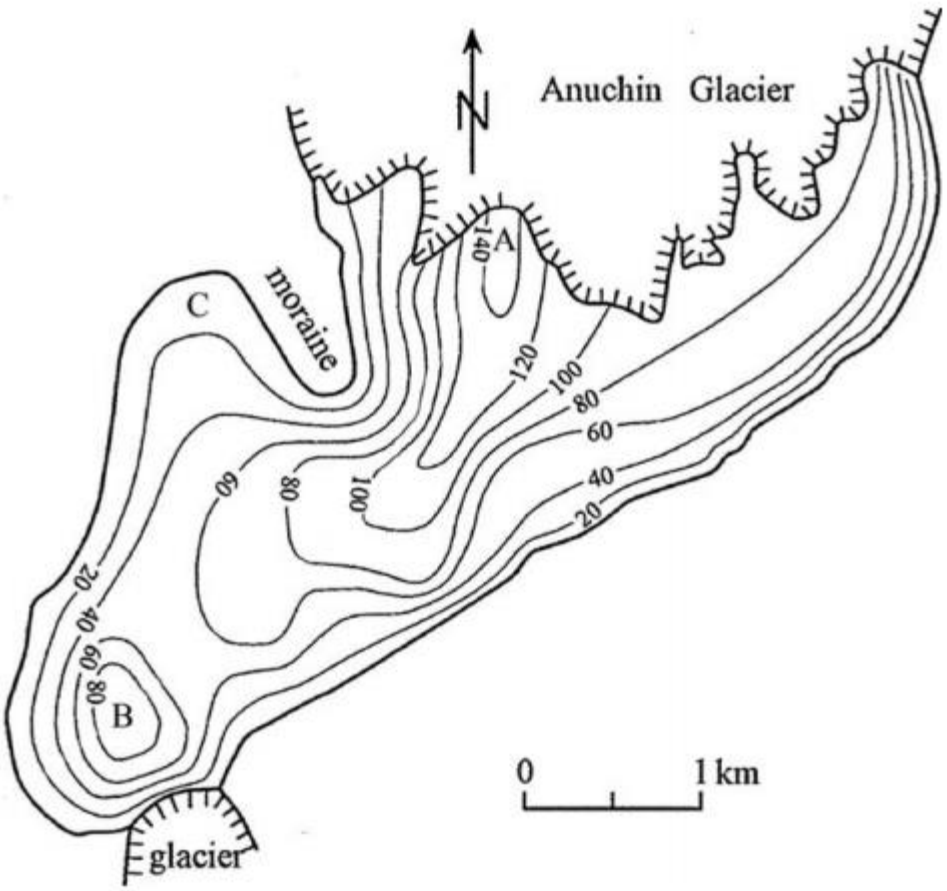

Figure 2. An outline of Lake Untersee showing its glacier boarders. The contours represent depth of the lake bottom from the surface. Image credit: Steel et al. 2015.

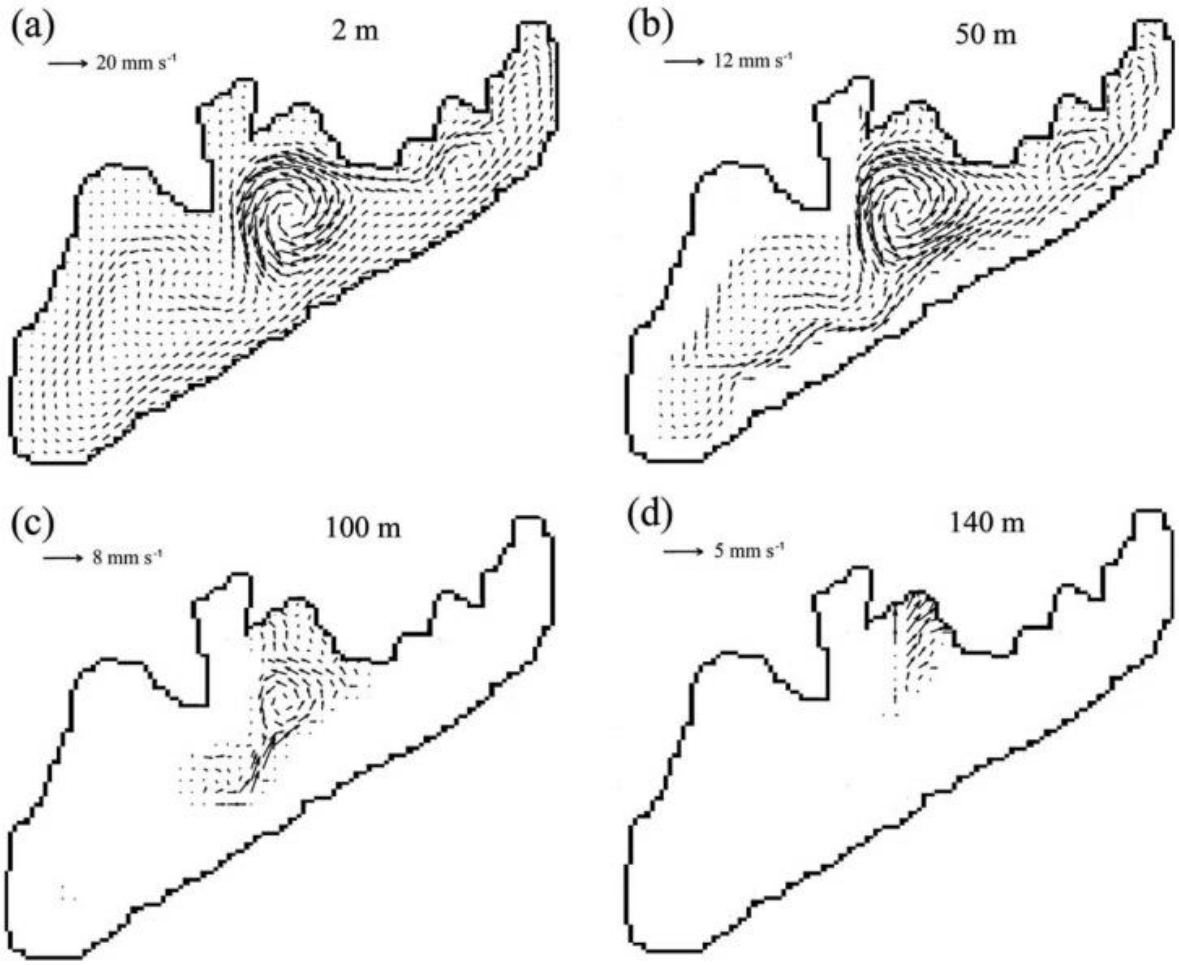

Figure 3. Each pane represents the horizontal currents at the noted depth. The currents are strongest at the top and decreasing with depth. Of major note are the relatively small currents in the southwestern anoxic region at 50m depth, and the nonexistent currents at 100m (3 nodes are pictured). Image credit: Steel et al. 2015.

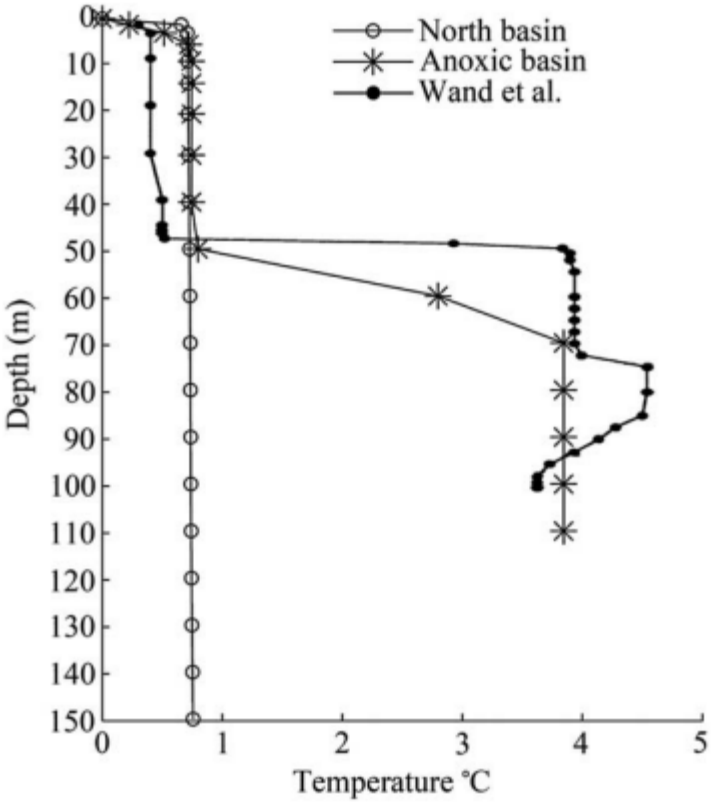

Figure 4. Neither of the expected thermal profile under the assumption of mixing dominated thermal heat transfer or diffusive heat transfer (not shown) account for the observed thermal bump between 65 and 95m. Image credit: Steel et al. 2015.

4. Thermal analysis

An analysis of the temperature is needed to provide boundaries to serve as guidance in identifying potential sources of thermal energy to explain the temperature bump. Temperature, pH, conductivity, oxidation reduction potential, dissolved oxygen and chlorophyll a profiles were measured in 2008 and 2011using a Hydrolab DS5 multi-parameter water quality sonde (OTT Hydromet, 5600 Lindbergh Dr., Loveland CO 80539). The profile was sampled at a resolution of 5m depths.

To understand the thermal sources, three approaches were conducted. The first is a simple, first cut approximation. The second two utilize the well-known heat diffusion equation in different ways. The first heat equation approach is an inverse method while the second is a direct or forward method.

The heat equation also known as Fourier's law is the predominant model of heat diffusion in a macroscopic classical physics framework. Similar to other diffusion principals, it illustrates that flux is inversely related to the driving pressure and that the medium acts to resist flux. Similar laws include Ohm's law of electrical conduction and Fick's law of particle diffusion. The 1d heat diffusion equation is given by

$$C_p \rho \frac{\partial T}{\partial t} = k \frac{\partial^2 T}{\partial x^2} + G(x,t)$$

Where T is temperature, t is time, x is the location given in Cartesian coordinates and $G(x,t)$ is a function in space and time describing the internal energy generation. Additionally, Cp, the heat capacity of the material, ρ,the material density, and k, the thermal conductivity of the material are assumed to be constant though they could be functions of space and time. Often, the equation is presented in a similar form

$$\frac{\partial T}{\partial t} = \alpha \frac{\partial^2 T}{\partial x^2} + G(x,t)$$

which is arrived at by dividing both sides by $C_p \rho$ and combining $C_p \rho / k$ into a new constant α which is known as the thermal diffusivity constant.

4.1. Steady state method

The first approach assumes constant conditions with time and constant temperature boundary conditions. Thus the analysis utilizes the simple heat conductivity equation

Q=k*(T2-T1)/(X2-X1)

where Q, heat flux, is the amount of thermal energy moving from one side of a uniform 1d block to the other, T2 and T1 are the temperatures at the ends of the block, the term X2-X1 is the thickness of the block, and k is a constant representing the thermal conductivity of the block material. A diagram of the system is given in figure 5.

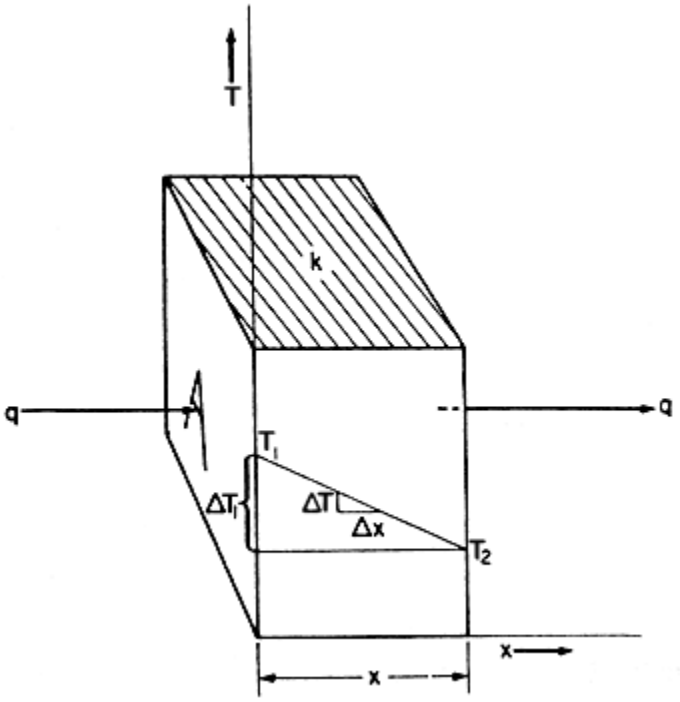

Figure 5. Diagram of a steady state uniform slab heat transfer. Image credit: Earle, 1983

Applying this equation to the temperature profile results in a rough estimate of the energy input required to maintain the thermal bump.

Assume: 3 sections
Left: Eloss from 4C at 65 m to 5C at 73 m
Center: Egen at 5C from 73 to 80 m
Right: Eloss from 5C at 80 m to 3.67C at 98 m

thus Loss_Left+Loss_Right=Egen_total
Loss=k*(T2-T1)/(X2-X1)
k=~0.6 W/(m*C)

Left:
Loss_Left=0.6*(5-4)/(73-65)
Loss_Left=0.075

Right:
Egen
Loss_Right=0.6*(5-3.67)/(98-80)
Loss_Right=0.0443

Egen:
Egen_total=0.119W

Assume: constant distributed energy generation
Egen_per_volume=Egen_total/(length_of_center*Area)
Egen_per_volume=0.119/(80-73)
Egen_per_volume=0.017 W/m3

From this analysis, a total energy input of 0.119W/m2 of lake area are needed to maintain the bump. Assuming that the energy generation is evenly distributed with depth between 73 and 80m the volume based generation would need to be 0.017 W/m3.

4.2 Inverse method

The second approach is an inversion method which consists of:

1. Setting parameters of interest such as the amount of energy generated and the location of the source
2. Using the heat diffusion partial differential equation (PDF) to predict the temperature profile
3. Then comparing the predicted to measured profile
4. Based on the error, parameters are changed
5. Iterations continue until the prediction match the measurements at which point the parameters of interest represent those of the actual system

To solve the PDE, a Crank-Nicolson scheme which is an implicit method and therefore always stable regardless of time step and space step sizes was implemented. The Crank- Nicolson scheme is a frequently used finite difference approach that improves on the accuracy of the forward and backward time step schemes. The forward and backward schemes are order one in error meaning that error scales linearly with node resolution. The Crank- Nicolson scheme on the other hand is second order meaning that doubling the resolution of the nodes results in a four fold reduction in error. Like the backward time step method, the Crank- Nicolson scheme is guaranteed to be stable for all time and space step sizes and combinations largely because it solves the nodes as a system of equations in a similar manner.

For this problem only the depths around the bump were modeled. The model included depths from 65m to 100m. Dirichlet boundary conditions i.e. constant temperature boundaries were applied to both the top depth and bottom depth. At the top, the temperature was held to 0C while the bottom was held at 4C. These values represent theoretical points and deviate slightly from the actual measurements. The initial conditions were set to a trapezoid approximating the shape of the profile. The model time was determined by assuming that there was no energy input then determining the point at which the model approximated a linear profile between the boundary conditions. Figure 6 illustrates the resulting plot. The time for the bump to fully dissipate was 190 years. A time step of 2.3 days and space step of 0.1m was used. These values were chosen because of their practicality. At this point in the analysis, it is more productive to be able to run the model quickly than spend too much time in an attempt to improve the accuracy of the model with smaller step sizes.

The system was used in two ways. First the depth range in which energy is assumed to be generated is constant and the program solves for the energy generation rate. For this analysis the range was assumed to be 73 to 80m. The models are evaluated by comparing the predicted temperature profiles to the measured profile through calculation of the mean square error (MSE). The results are summarized in table 1. It can be seen that a minimum error occurs at an energy generation rate of 0.0138 W/m3. This is equivalent to 0.091W total which is very similar to the results of the steady analysis above. The second assumes a constant energy generation rate but solves for the best range for which energy is generated. The results are summarized in table 2 and depicted in figure 8. The range of 72 to 83m has the lowest error. This range is very similar to the one assumed above.

Despite the agreement with the results above, there are some major discrepancies as seen in figure 7. In particular, the measured upper profile segment is much steeper than the predicted one and the measured profile is much flatter in the bump than the predicted profile. This suggests that there is something missing from the model as it does not accurately reproduce the shape of the profile.

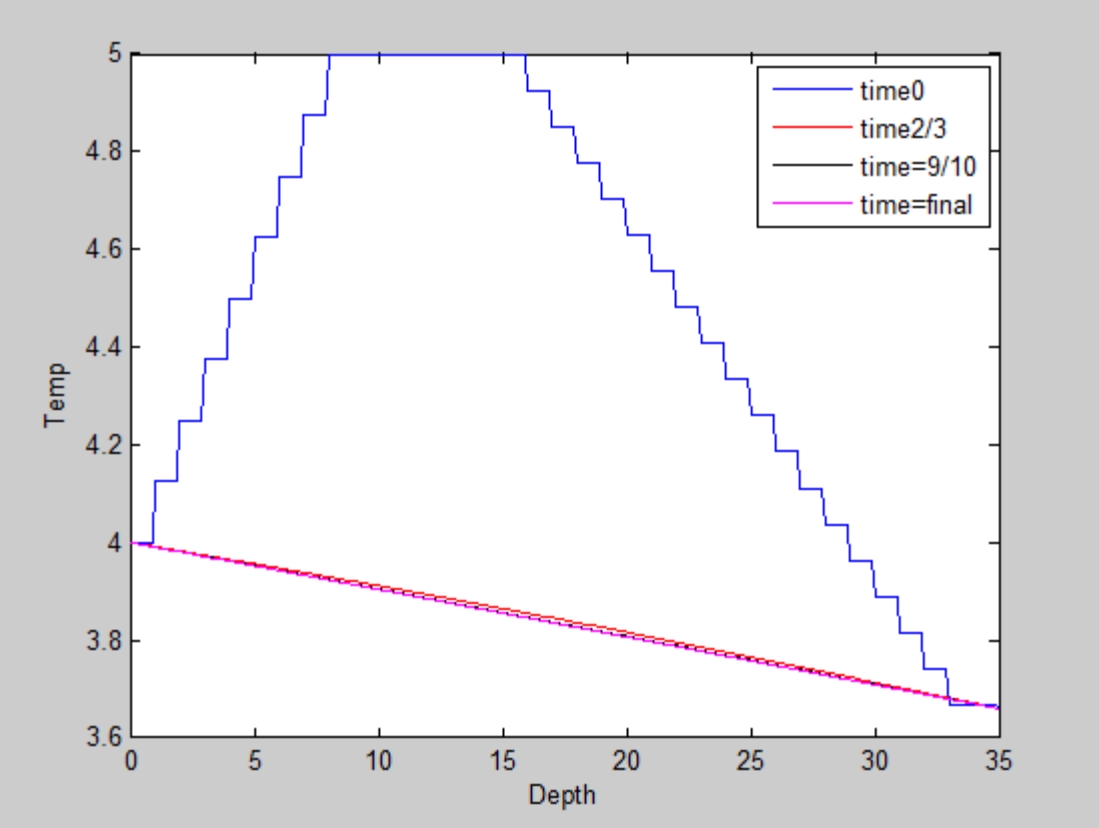

Figure 6. Plot of temperature if there were no energy generation. The blue line represents the initial conditions. By 90% of the simulation, the temperature id fairly stable as it does not deviate much from the final profile which occurs at 190 years of simulation.

Table 1. Mean square error of models with different energy generation values

Egen (w/m3)	MSE
0.000001	0.590
0.00001	0.589
0.0001	0.581
0.001	0.509
0.01	0.054
0.011	0.034
0.012	0.020
0.013	0.012
0.0131	0.012
0.0132	0.011
0.0133	0.011
0.0134	0.011
0.0135	0.011
0.0136	0.010
0.0137	0.010
0.0138	0.010
0.0139	0.010
0.014	0.010
0.015	0.015
0.016	0.025
0.017	0.042
0.018	0.065
0.019	0.094
0.02	0.129
0.1	22.722
1	2971.207

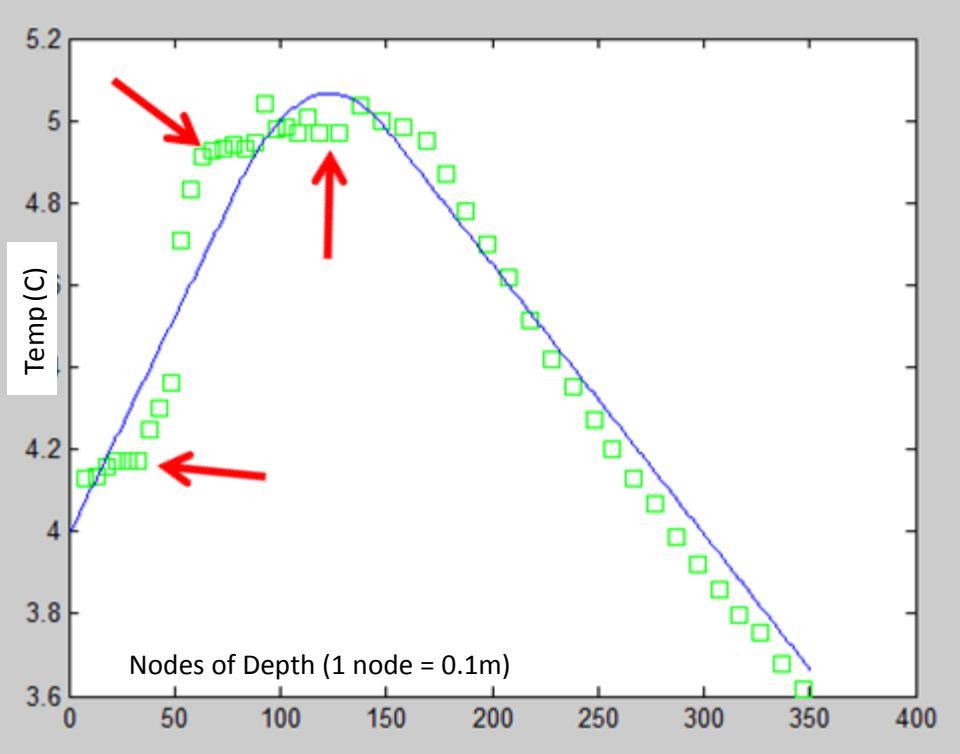

Figure 7. The green points represent the measured profile and the blue line represents the predicted profile. The predicted profile does not match the measured profile well.

Tabel 2. Mean square error of models under different assumed energy generation ranges.

Range		MSE
67	77	0.306
67	78	0.296
67	79	0.291
67	80	0.287
67	81	0.286
68	78	0.205
68	79	0.194
68	80	0.187
68	81	0.183
68	82	0.183
69	79	0.126
69	80	0.114
69	81	0.107
69	82	0.105
69	83	0.105
70	80	0.068
70	81	0.058
70	82	0.052
70	83	0.051
70	84	0.054
71	81	0.030
71	82	0.023
71	83	0.021
71	84	0.022
71	85	0.027
72	82	0.012
72	83	0.010
72	84	0.012
72	85	0.017
72	86	0.025
73	83	0.012
73	84	0.016
73	85	0.024
73	86	0.035
73	87	0.047

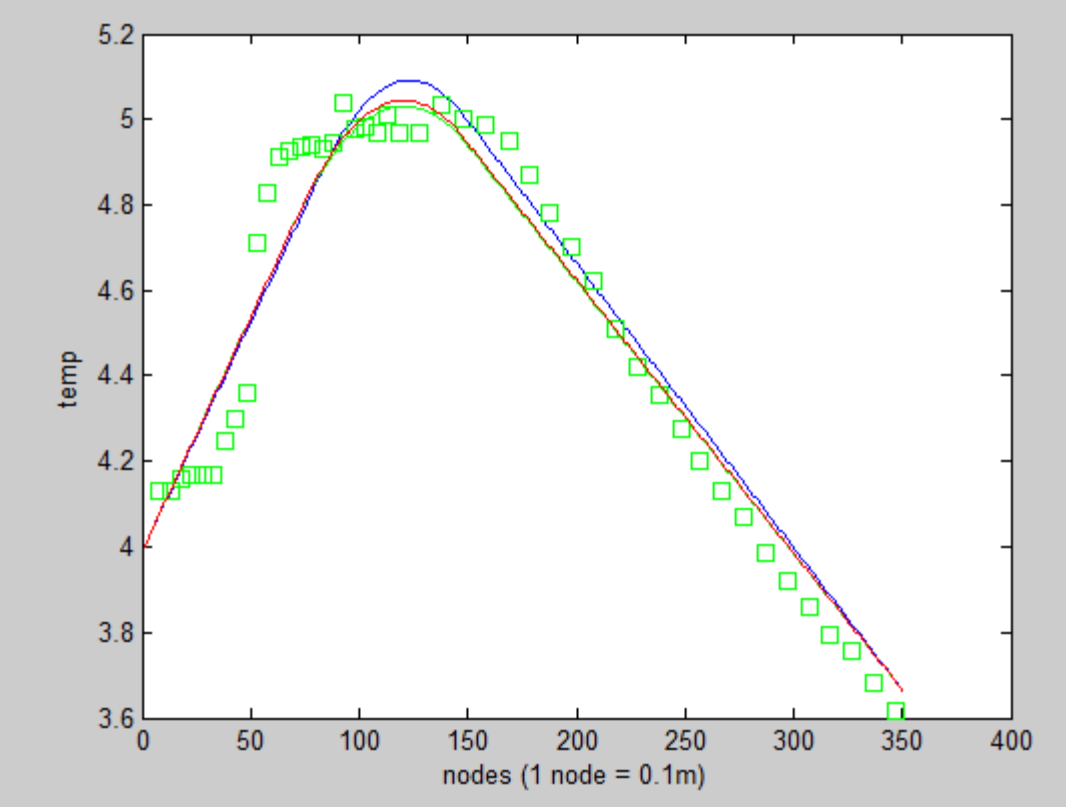

Figure 8. Plot of predicted temperature profiles resulting from changing the assumed energy generation ranges. The colors of the profiles represent the models highlited in table 2.

4.3. Direct method

The third approach leverages a rearranged version of the heat equation to isolate the energy generation term. The steps required for this rearrangment require an assumption about the term $\frac{\partial T}{\partial t}$. For this analysis, it is assumed that $\frac{\partial T}{\partial t}$ is 0. Thus

$$C_p \rho \frac{\partial T}{\partial t} = 0 = \alpha \frac{\partial^2 T}{\partial x^2} + G(x)$$

where the internal energy generation term in now only a function of space and not time. Rearranging yields

$$G(x) = -k \frac{\partial^2 T}{\partial x^2}$$

for which the right hand term, $\frac{\partial^2 T}{\partial x^2}$ can be solved numerically from the measured temperature profile and multiplied by *-k*.

The second derivative of the profile was approximated using the centered, second derivative formula

$$f''(x) \cong \frac{f(x+h) - 2f(x) + f(x-h)}{h^2}$$

where h is the distance between node steps. This formula is second order in regards to error. However, the resulting profile is much noisier than anticipated as seen in figure 9. The major surprise here is the presence of a negative spike at 4 m corresponding to a depth of 69 m. To verify that the calculation was correct, the approximated energy generation function was used as input into the Crank-Nicolson model. Figure 10 is the resulting profile which is nearly identical to the measured profile. Thus, the calculation is confirmed to have been correct.

However, it appears that the positive area between 5 and 9 m may be enough to offset the negative peak. In an attempt to reduce noise, a moving average was applied to the G(x) approximation. This produced a cleaner profile but the negative spike still persists. Figure 11 shows a profile that was smoothed with a moving average window of 5. As a second smoothing attempt, a moving average was applied to the temperature profile prior to numerical derivation to see if this improved the results. Figure 12 shows the results from a moving average window of 5. Again, the negative spike is present and the profile looks very similar to the profile where the moving average was applied after numerical derivation. Thus, the spike may not be an artifact of numerical analysis. Looking back at the heat diffusion equation reveals some clues. The sign of the energy generation is opposite to the sign of the curl of the temperature function at that location. At 4 m (64 m lake depth), there is a positive curl where the function turns upward. This is the source of the peak from a numerical sense. In real world terms, this likely represents a flux boundary equation that arises from slight mixing that may be occurring at the interface.

Regardless of the negative spike, the results are largely too noisy to be informative. It is difficult to tell which peaks are numerical artifacts and which are actual sources. Thus, the results are largely inconclusive.

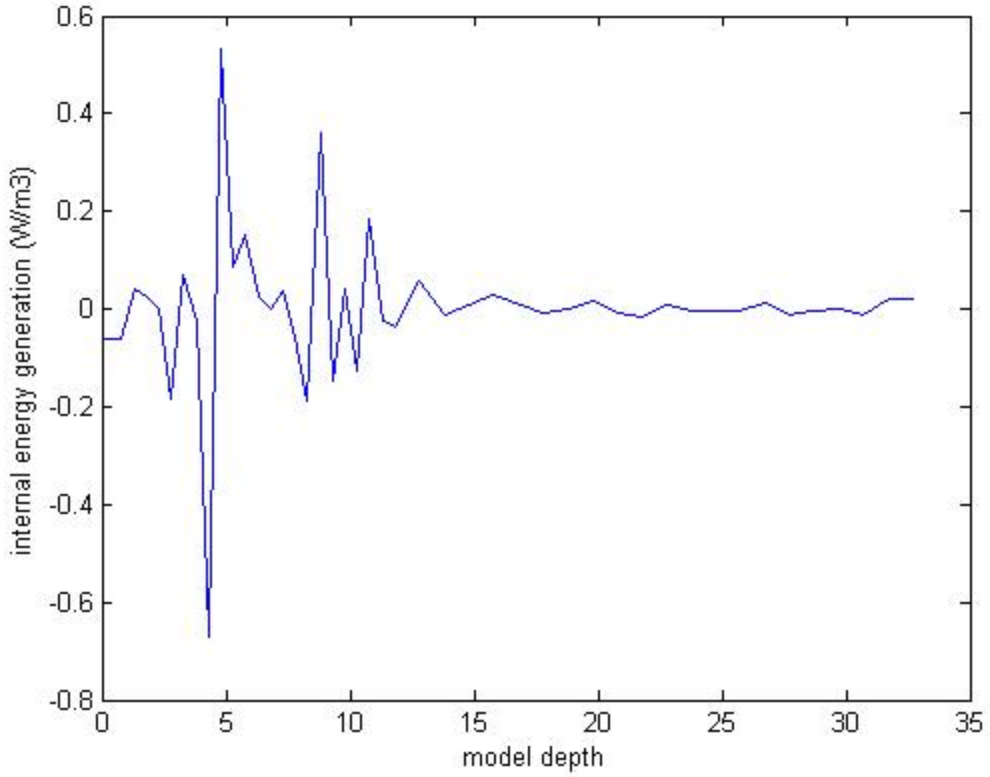

Figure 9. energy generation profile derrived numericaly from the measured temperature profile. The sharp negative peak at 4m is a surprising result. The depths given on the x axis are translated such that 0m is equivilant to 65m of depth in the lake water column.

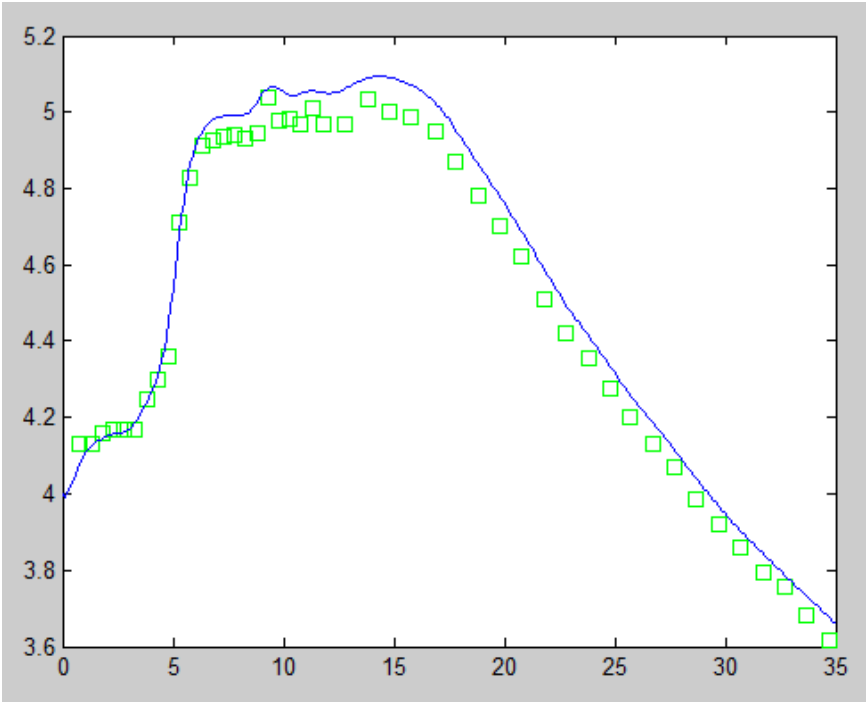

Figure 10. confirmation of the energy generation function calculation. The numericaly derrived results were used as input into the diffusion model. The profiles are very similar and the descrepencies are likely from numerical information loss.

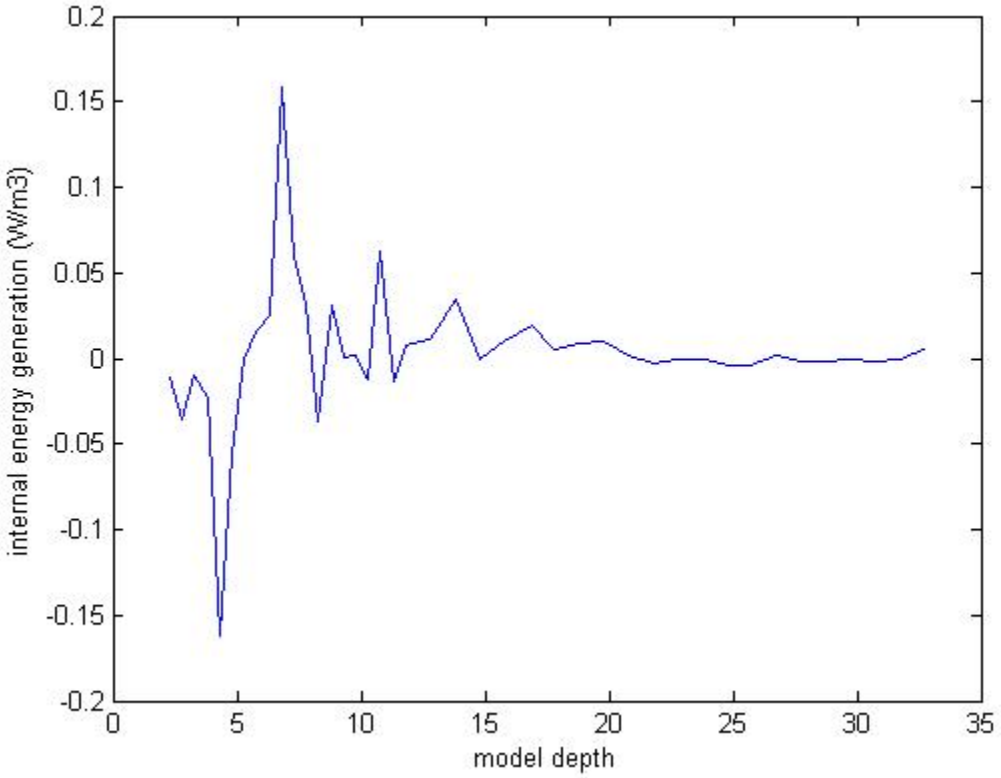

Figure 11. numerically derrived energy generation function with smoothing. This profile was smoothed using a moving average window of 5. This reduced noise but the negative peak at 4m persists.

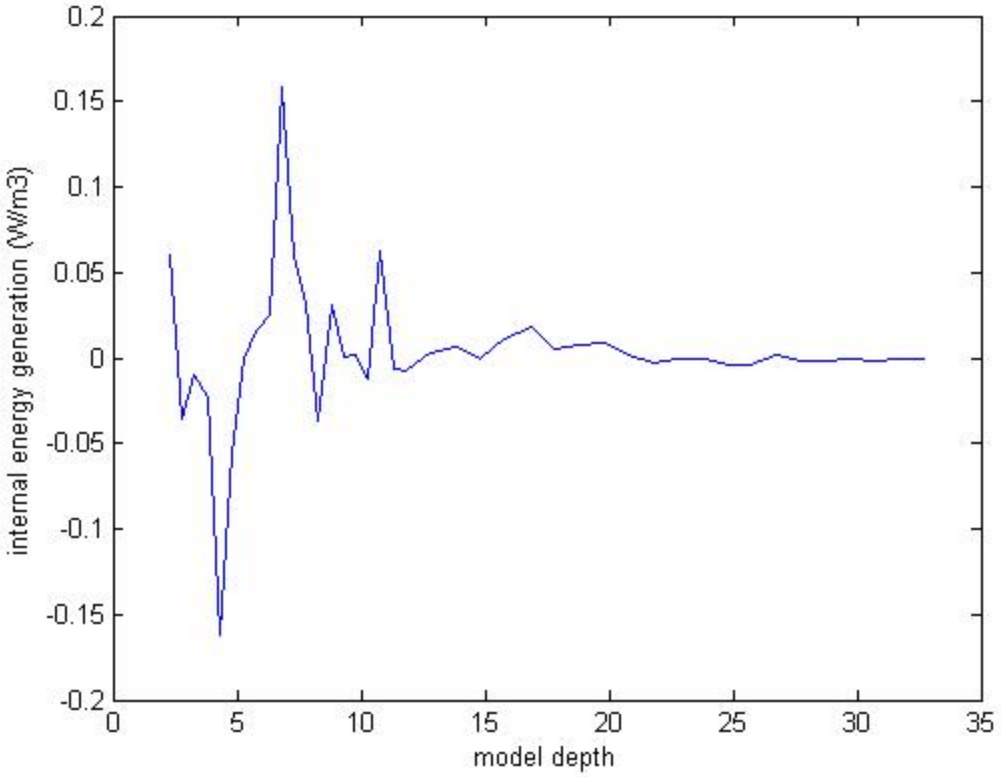

Figure 12. energy function numerically derrived from a smoothed temperature profile. This profile was smoothed using a moving average window of 5. This reduced noise but the negative peak at 4m persists.

4.4. Linear approximation

Since the data was too noisy to produce a reliable energy generation function, a simpler approach was needed. The approach should be derived from the measured data but also need to be simple and reliable. Thus, a hybrid approach was taken. Instead of using each measurement, the profile was broken into sections. Each section is then approximated using a regression line. Together the lines approximate the profile but greatly simplify the analysis by reducing noise. With the estimated profile, direct method calculations can be made. This analysis was conducted on 2 datasets 2008, and 2011.

The segments and their respective regression lines are shown in figure 13 and figure 14. The profile is best estimated by breaking the profile into 4 portions. Of the 4 portions, only 3 of them will be used in analysis. One portion is rejected because it represents the section believed to be caused by slight mixing or a boundary condition (only shown in figure 13). To remove this section is to effectively assume that the new boundary is within that portion. This is fine for the analysis because it doesn't contain the portion of the water column that we are interested in anyway. The regression lines fit the left (top) and right (bottom) segments of the measured profile very well as measured by the R2 value which is greater than 0.9. On the 2008 data, the middle segment however, has a much lower R2 of 0.46. This segment has some noticeable points which deviate from the line. Methodically removing points reveals that the regression line is not strongly effected by theses points because the slope and intercept values don't

change much. However, when these points are absent, the R2 value increases greatly. For example, removing the obvious point in the middle results in a slope of 0.0124 and R2 of 0.78. Since the line is basically the same, the points will be left as there is no strong argument to support removing them.

Using the mathematical properties described in the Direct Method section, the profile can be used to approximate the energy generation function. Since the profile is now reduced to a series of lines, the analysis becomes very simple. The location of the heat sources is simply the intersection points between the lines. The flux in each section is the slope of the line of that segment time k and the magnitude of the energy generation source is equivalent to the change in slope between the lines.

The left and right lines represent energy flux leaving the system. Thus to remain in steady state, the sum of these 2 fluxes must be replaced. For the 2008 data the total energy requirement is 0.202 W/m2. Source 1 is a point source of 0.153 W/m2 located at 71.13 m while source 2 is a point source of 0.049 W/m2 located at 80.67 m. For the 2011 data, the total energy input is 0.118 W/m2. Source 1 is 0.719 W/m2 at 71.39 m while source 2 is 0.046 W/m2 at 80.45 m. The location of both sources is very stable between the 2 years and the energy input of source 2 is also stable. However, the energy input of source 1 is much more variable being twice the magnitude in 2008 as 2011. This likely arises from the steep slope of this segment. The measurement resolution is on the verge of being under sampled and small errors in depth accuracy can result in large slope changes. These are probably the reason for the variability in the estimates of source 1. To reduce inaccuracy, the results from the 2008 and 2011 data will be averaged to leverage the central limit theorem. This results in a source 1 of 0.113 W/m2 at 71.26 m and a source 2 of 0.048 W/m2 at 80.56 m. A summary of the sources is presented in table 3.

Table 3. summary of energy sources

2008	Depth	Energy
S1	71.13	0.153
S2	80.67	0.049
Sum		0.203

2011	Depth	Energy
S1	71.39	0.072
S2	80.45	0.046
Sum		0.118

Mean	Depth	Energy
S1	71.26	0.113
S2	80.56	0.048
Sum		0.160

0.16 W/m2 is higher than the estimates of 0.119W/m2 and 0.091W/m2 found above. The primary reason for this change is the exclusion of the upper segment which represents a major thermal sink. Thus, the new energy estimate includes not only the energy sources but also the energy flux at the

boundary. From the direct analysis above, the boundary flux is at least on the same order of magnitude as the energy required to maintain the temperature bump. Another significant result of this analysis is that it demonstrates the presence of two thermal sources instead of one. One distributed source could never produce the boxy profile that is observed. As seen above in the inversion section, a distributed source produces a parabola shaped profile. The assumption of a distributed source is natural because it is the simplest structure and the profile provides natural ranges between the corners. However, for two sources, the profile doesn't offer much to guide the selection of ranges because the middle section is featureless. Guessing the ranges and source magnitudes as was done in the inversion section for two sources would be complicated and the results would be less convincing. The results of this section will be used in the following section to guide and restrict the search for physical energy sources.

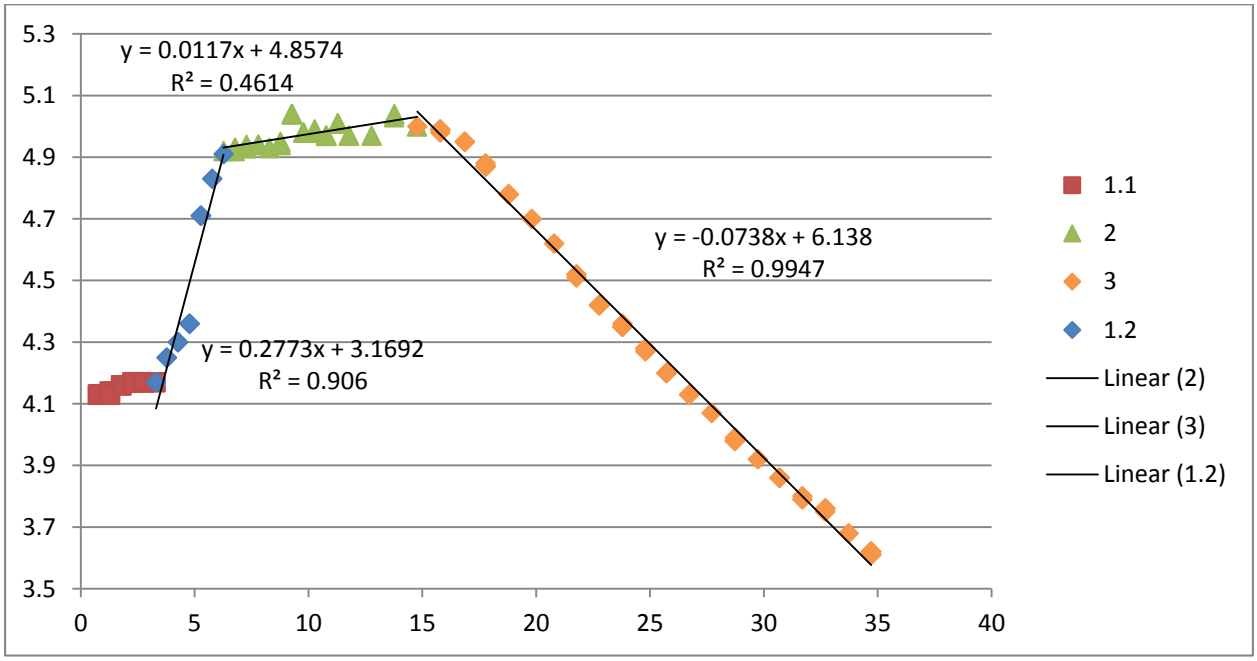

Figure 13. Linear regression lines fit to the 2008 data to approximate the profile. The lines facilitate easy calculations, remove noise, yet still represent the measured profile. The points in red are discarded from the analysis

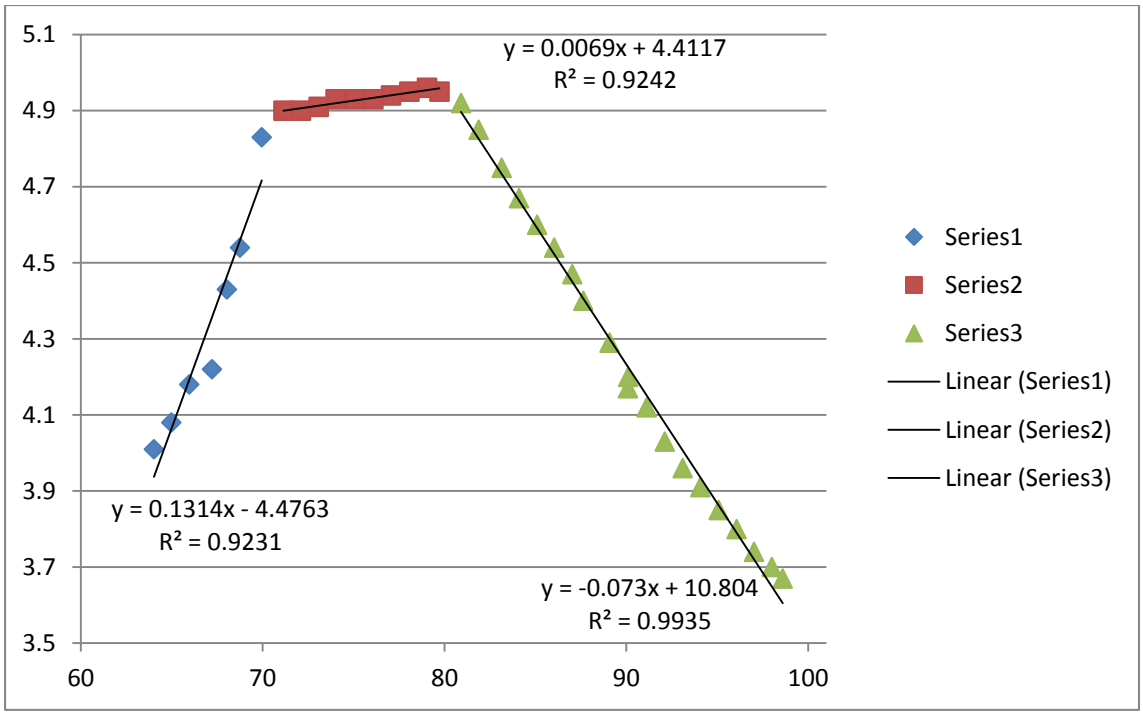

Figure 14. Linear regression lines fit to the 2011 data to approximate the profile. The slope of the left leg differs from the slope in figure 13 of the 2008 data.

5. Energy Sources

From the thermal analysis, the characteristics of the thermal sources have been estimated. However, the sources currently have no tangible meaning. The goal in the section is to find a physical mechanism to explain the thermal energy input. Potential sources include chemical reactions, biological metabolism, and radiative energy.

5.1. Chemical and biological reactions

From Wand et al. 2006 it is well known that there are several species of chemicals in the water column with some at relatively high concentrations. Thus the possibility that chemical reactions are occurring between some species in the water column is high. Additionally, many of the chemicals found in the water column are known to be energy sources or nutrients that support life or by products of metabolic reactions. Wand et al. 2006 asserts that there is an active ecosystem of microorganisms which collectively carry out a variety of reactions metabolically. As metabolic reactions, they should be exothermic meaning that they give of energy as a product of the reaction.

Prior to investigating the chemistry, it is important to understand the environment and condition of the water. Basic measures like pH and oxidation reduction potential (ORP) can be very informative. Normalized profiles of some environmental parameters are shown in figure 15 with respective scaling factors in table 4. At about 70 m there are some sharp changes in the water properties. In particular, pH drops and ORP increases. These actions coincide with a sharp drop in dissolved oxygen marking the oxycline. At a depth of about 76 m, ORP starts a sharp decline reaching a lower boundary by 85m of

depth. This shift in ORP marks changes in the types of chemical reactions that are likely to occur. It may also be linked to the suboxic determination given by Wand et al. 2006 of the column between 70 and 80m with the shift representing the boundary to fully anoxic. It is also important to note the increase in conductivity starting at 80 m and climbing to the bottom of the lake.

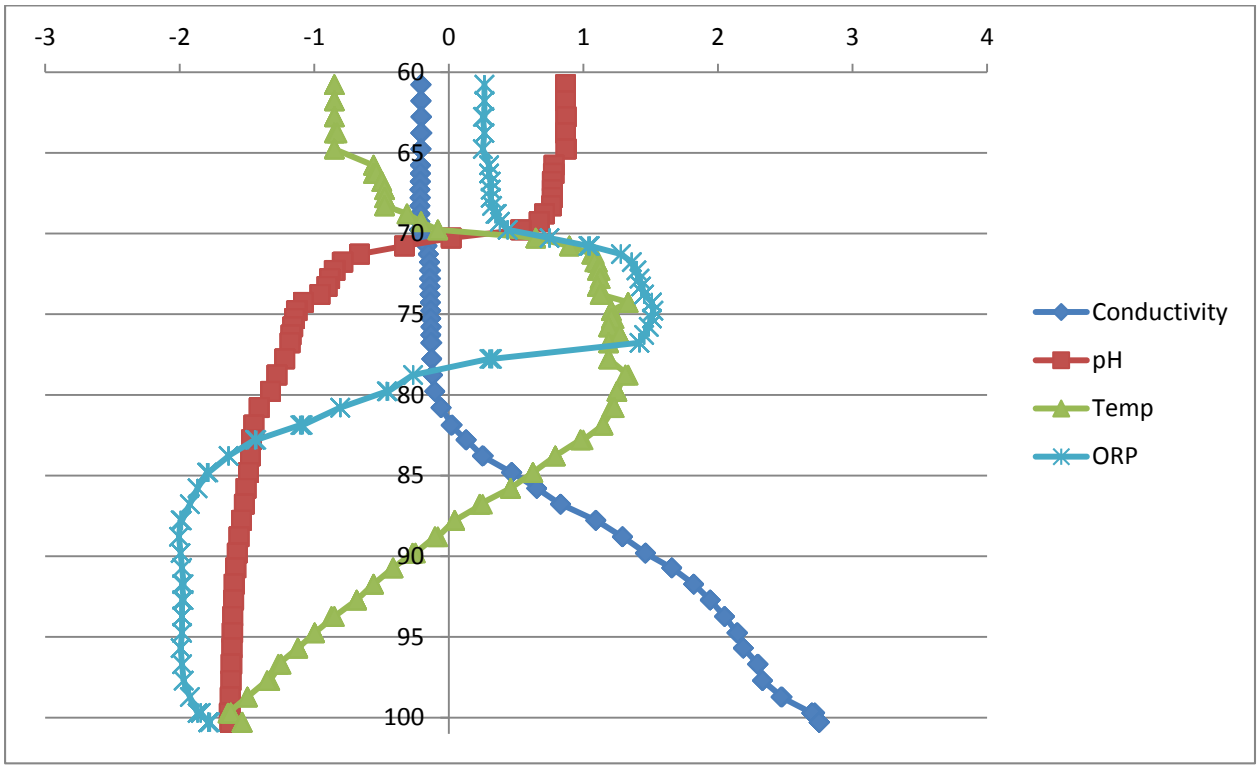

Figure 15. Profiles of water environmental parameters. All variables have been normalized to show the relative values of the profiles. The scaling factors are given in table 4.

Table 4. scaling factors for variables in figure 15.

	Temp C	pH Units	ORP mV	SpCond µS/cm
Mean	4.399	9.234	207.043	585.298
Std Dev	0.481	1.529	86.790	308.747

Now looking at the chemicals more specifically, Wand et al. 2006 has conducted the most thorough inventory of chemical species to date. Table 5 is the raw chemical concentration measurements given by Wand et al. 2006. Additionally, Wand et al. 2006 provides a graphical profile of Ammonium but the measurements were not included any of the tables and is reproduced in figure 16. Of particular note is the increase in organic and inorganic species starting at 80 m and increasing with depth to the bottom. This reflects the same pattern as conductivity. Conductivity is used a surrogate for dissolved solids in the water. In highly saline water it can be used to estimate the salinity of the water because the other dissolved solids make up only a minor fraction in comparison to the approximately 3.5% salt content. In the context of Lake Untersee which is among the freshest water in the world, the conductivity measure

should represent the non-saline component well which is a luxury not often afforded. The high concentration of methane is also important because methane is an important component of the carbon cycle providing strong indication that there is an active ecosystem.

Table 5. Chemical profiles from Wand et al. (2006)

Depth (m)	SO4 (g/L)	CH4 (g/L)	DO (mg/L)	DIC (mg/L)	DOC (mg/L)	POC (mg/L)
10	163.4	BLD	19.301	6	0.58	0.007
20		BLD	19.035			
30		0.15	18.183	0.008	4.29	
50	167.7	0.45	20.247	7	0.66	0.009
70	165.2	0.65	11.528	3	0.61	0.010
71				8	0.74	0.010
72				6	0.51	0.009
73				2	0.78	0.013
74	161.9	1.15	1.524	23	0.97	0.016
75	160.2	1.49	0.353	28	1.09	0.030
76	165.2	1.85	0.287	24	1.00	0.019
77				25	1.07	0.025
78	162.4	3.50	0.240	25	0.95	0.018
79				23	0.97	0.006
80	159.5	10.20	0.240	25	0.98	0.012
82				45	1.15	0.026
84	63.8	2,850	0.240	227	3.28	0.030
85	68.2	4,900	0.238			
86	73.0	5,300	0.230	228	3.52	0.020
88				332	4.52	18.320
90	48.1	10,200	0.230	439	6.23	0.021
92	25.5	12,350	0.230	474	7.02	26.800
94	16.8	15,850	0.220	535	7.26	0.035
95	16.8	17,800	0.220			
96	15.2	17,950	0.217	574	7.97	0.231
98	29.1	19,700	0.210	560	8.71	0.483
99	14.8	21,800	0.213	679	13.50	1.271

BDL is below detection limit

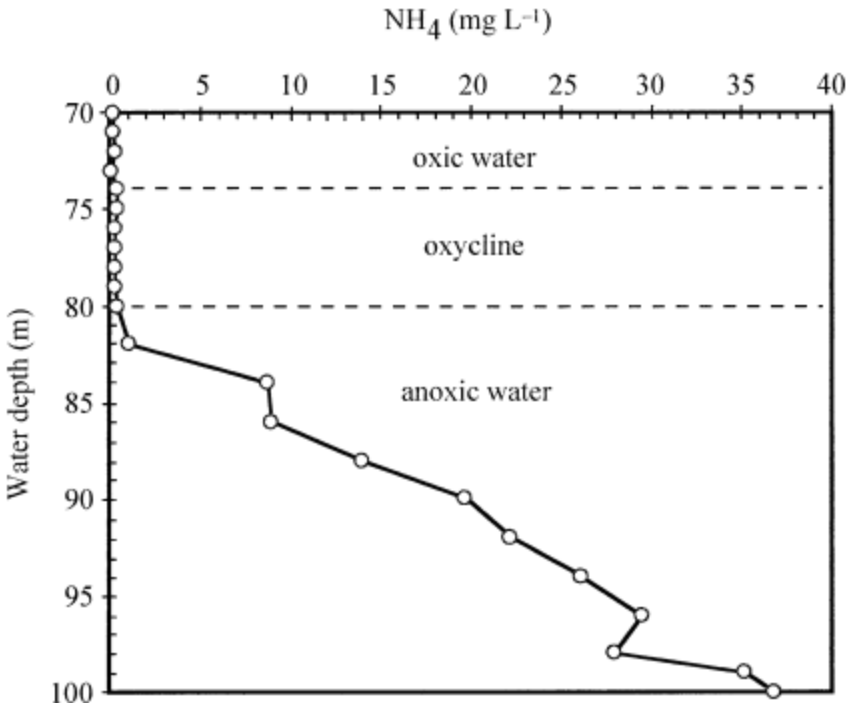

Figure 16. Ammonium profile from Wand et al. (2006). This data was not provided in the chemical table of Wand et al. (2006).

As a first analysis, biological reactions will be treated as chemical reactions. The main difference between the two for this analysis is that biological reactions are converting a portion of the energy derived from the reaction into other chemical bonds. This fraction would ultimately reduce the amount of heat produced. Also, estimating the portion that results in heat is an analysis in it on right and should only be added if proven necessary. Wand et al. 2006 suggests some reactions that are likely occurring in the water column which are given in figure 17. Table 16 also contains the associated upper limit of energy release from these reactions. In Wand et al. 2006, there is an experiment which suggests that reaction 1 is not a primary reaction and that reaction 2 is more common. Of the reactions, reaction 3 produces much more energy than the others. Reactions 1 and 4 are an order of magnitude smaller that reaction 3 in energy production. Potentially there are other reactions not identified by Wand et al. 2006 but these are used as a starting point.

$$CH_3COOH \rightarrow CH_4 + CO_2 \quad (1)$$

$$4H_2 + CO_2 \rightarrow CH_4 + 2H_2O \quad (2)$$

$$CH_4 + 2O_2 \rightarrow CO_2 + 2H_2O \quad (3)$$

$$CH_4 + SO_4^{2-} \rightarrow HCO_3^- + HS^- + H_2O \quad (4)$$

Figure 17. Suggested metabolic reactions from Wand et al. (2006)

Table 6. Upper limit energy release from potential reactions

Reaction #	Energy Release (kJ/mol)	Source
1	33	Milo et al. (2010)
2	135	Milo et al. (2010)
3	802	CRC (1976)
4	25	Reeburgh (2007)

The chemical analysis is very similar to the thermal analysis because the equations are nearly identical and the known portions i.e. the driving force, are known. The model used for chemical diffusion is given by Fick's law

$$\frac{\partial \phi(x,t)}{\partial x} = D\frac{\partial^2 \phi(x,t)}{\partial x^2} + C(x,t)$$

where $\frac{\partial \phi}{\partial x}$ is the chemical flux, D is the diffusion constant, $\phi(x,t)$ is the chemical concentration and a function of space (x) and time (t), and $C(x,t)$ is a term to describe consumption and generation of the chemical species. Like with the thermal analysis, a curved profile suggests chemical generation or consumption and a strait profile suggests the absence of a reaction. This signature provides a criterion for estimating the locations of chemical reactions.

The first chemical species investigated is methane. Methane was chosen because it has an easily interpretable chemical profile, is present in high concentrations, and contains lots of energy. The methane profile measured by Wand et al. (2006) is given in figure 18. The profile can be broken into three segments. The top segment is the upper column which will be ignored. The middle segment is between 70 and 80 m. In this segment, the profile is curved in a concave fashion suggesting that there is methane consumption. The last segment is from 80 m to the bottom. This segment is mostly linear implying that there is no consumption or production in the region.

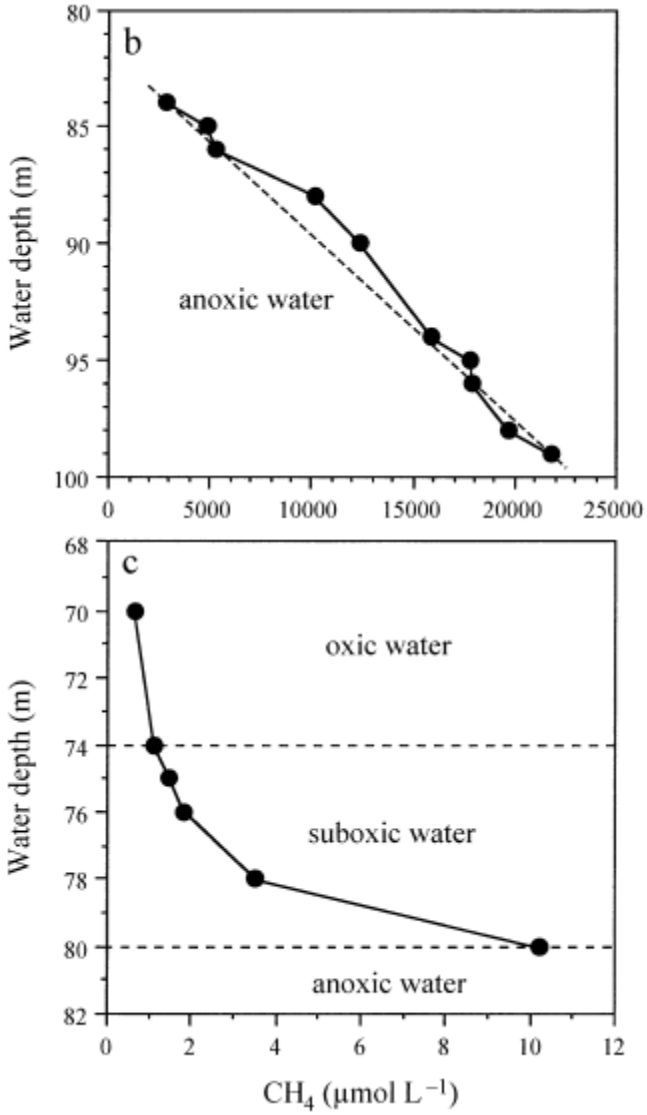

Figure 18. Methane profiles from Wand et al. (2006). The segment from 70m to 80m is concaved suggesting that there is methane consumption. The segment from 80m to the bottom is mostly linear implying that there are no reactions involving methane at these depths.

5.1.1. Direct approach

A direct method similar to the one used in the thermal analysis can be applied to the profile by assuming that $\frac{\partial \phi}{\partial x}$ is 0.

$$\frac{\partial \phi(x,t)}{\partial x} = 0 = D\frac{\partial^2 \phi(x,t)}{\partial x^2} + C(x,t)$$

Then rearranging the equation gives

$$C(x) = D\frac{\partial^2 \phi(x,t)}{\partial x^2}$$

where the right hand term can be solved numerically from the profile given in table 5 using the centered finite difference second derivative equation. The results from this technique applied to the methane profiles were extremely noisy as seen in figure 19. One important outcome is that the reaction rates are very small.

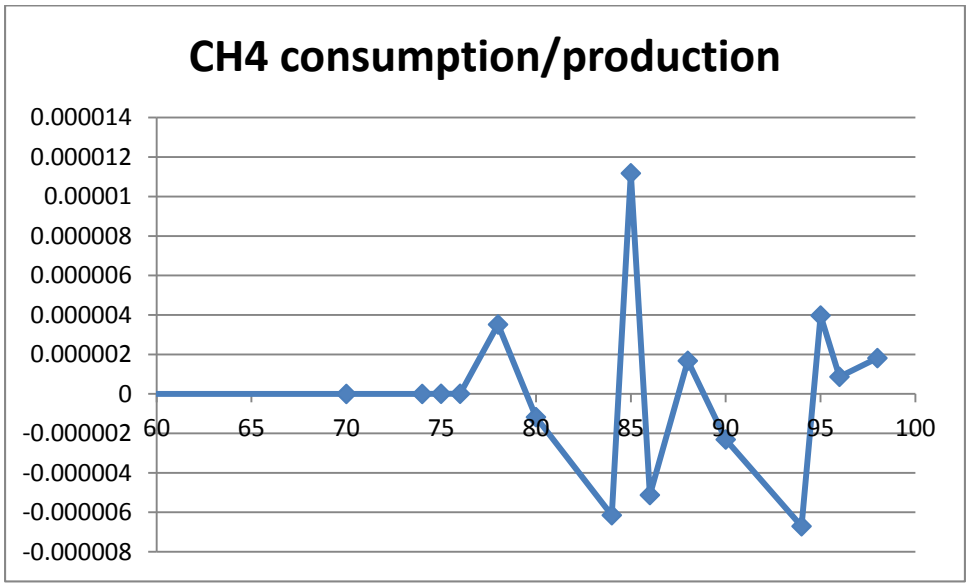

Figure 19. Consumption/production profile of CH4 as determined by taking the second order derivative of the methane profile, the results are very noisy and difficult to interpret.

5.1.2. Hybrid approach

In an effort to improve on the numerical results, an approach similar to the hybrid approximation used in thermal analysis was applied. This effort consisted of fitting different curves to the measured profile. Figure 20 shows profiles of oxygen and methane. The curves in the plot are the closest approximations achieved. Both have high R2 values but this is discarded as a relevant indication because there are relatively few points in the profile and complex equation can easily over fit the data producing a falsely accurate fit. More important is the fact that the curves deviate from the measured profiles in several places. Thus, it appears that fitted curves will not approximate the profile well. The analysis likely fails because the profiles are more complex and the measured data is much too sparse to describe the complexity.

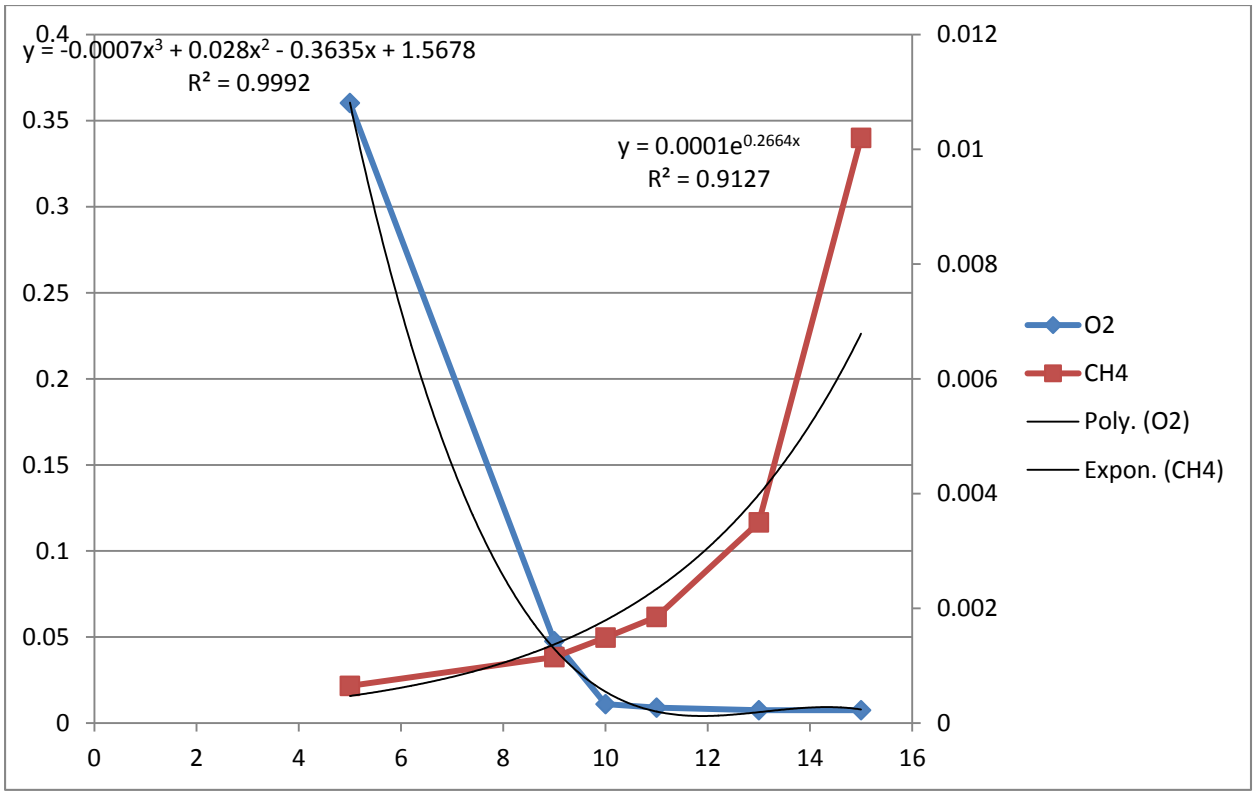

Figure 20. Fitted curves to measured profiles of two chemical species. The curves produce high R2 values but ultimately don't fit the measured profile. The high R2 is likely a reflection of overfitting a complex curve on a small number of measurements. Data from Wand et al., 2006

5.1.3. Simplified approximation

Given that the chemical consumption rates appear to be small, it is important to verify that further time investment in determining accurate and precise values is relevant. In other words, the values are only important if they contribute substantially or in part to the energy required to produce the thermal profile. As a very rough approximation, the segment from 70m to 80m was treated as a single unit. Thus, the methane consumption into the unit is equivalent to

$$Consumption = CH4\ flux\ out - CH4\ flux\ in$$

where each flux, J, can be approximated for methane by

$$J = -D\frac{\partial \phi}{\partial x}$$

where $\frac{\partial \phi}{\partial x}$ is estimated from the slope of the concentration profile as seen in figure 21. Assuming that there is no flux out, and that the reaction is not limited by oxygen, the energy produced is

Reaction Rate:
Flux_in = D*slope_in
D = 0.95e-9 m2/s at 5C
Slope_in = 1.204 mol/m2

Flux_in = 1.14e-9 mol/s

Energy production:
Delta_G_of_reaction = 800 kJ/mol
Energy = mol_of_reaction * Delta_G_of_reaction
Energy = 1.14e-6 mol/s * 802 kJ/mol
Energy = 9.81e-4 W

This reaction is 0.6% of the needed energy. Given the small value, the energy contribution is negligible compared to the required source. Moreover, if this is a biologically mediated reaction, the heat production will be much less. As methane oxidation is expected to produce the most heat of all of the reactions, it is assumed that the others, even if combined, are also negligible.

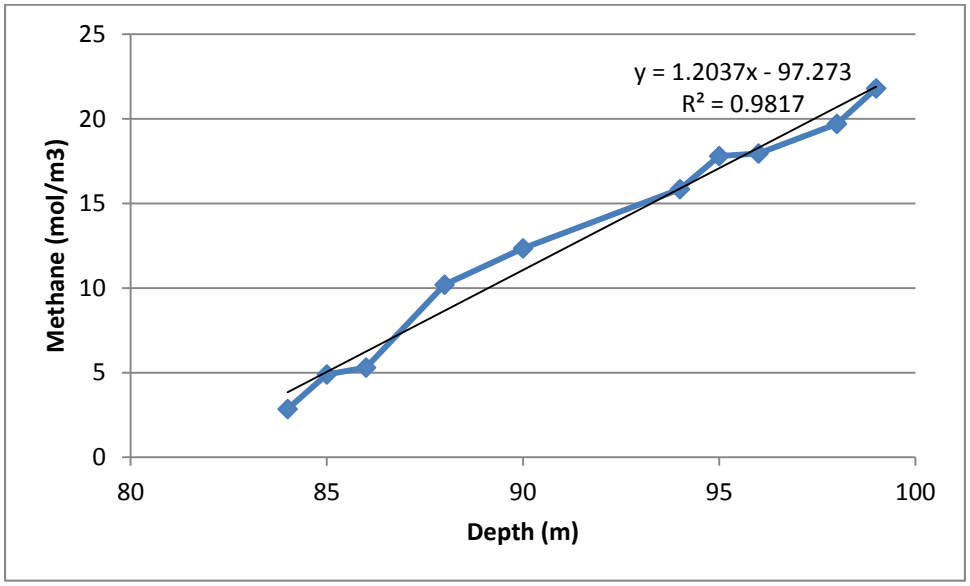

Figure 21. Fitted line to the bottom segment of the methane profile. The slope can be used to estimate the methane flux. Data from Wand et al., 2006.

5.1.4. In vitro rates

One set of experiments conducted by Wand et al. 2006 measured the reaction rates of various reactions in the lab. The measurements looked at specific species in vitro to determine their production or consumption rates. This was conducted with samples from different depths to approximate a profile. The species were methane and sulfate and the reactions were methane production (MPR), methane oxidation (MOR), and sulfate reduction (SRR). The results are given in table 7. The highest reaction rate for methane oxidation is 2.12e-8 mol/m3/s resulting in 0.0189 W/m3 of energy production. This is similar to the production rates predicted above if the total energy input is spread across the 7m width of the thermal bump. In other words, 0.160 W/m3 divided by 7m which is 0.0229 W/m3. However, the rate measured by Wand et al. 2006 occur across only 1-2m and thus is not capable of producing the required 0.160W/m3. Moreover, the rates presented by Wand et al. 2006 are for in vitro measurements. In vitro measurements are easily 2 orders of magnitude larger than in vivo rates and thus don't represent the

absolute energy production well. What is interesting about the rates presented in Wand et al. 2006 is the relative values. In the zone from 80 to 85 m both methane oxidation rates and sulfate reduction rates reach maximum values. Methane production rates in the water column reach a maximum at 90 m.

Table 7. In vitro reaction rates from Wand et al. (2006)

Depth (m)	MPR(CO2) nmol/L/D	MPR(Acetate) nmol/L/D	MOR µmol/L/D	SRR µmol/L/D
70			0.006	
71	0.250	0.031	0.009	0.0016
73	0.833	0.025	0.010	0.0031
74	1.665	0.020	0.052	0.0094
75	1.665	0.017	0.020	0.1466
76	21.647	0.027	0.260	1.8341
80	439.600	0.033	0.31	0.0025
85	53.285	0.059		0.0012
86	22.480	0.082		0.0006
88	56.615	0.061		0.0003

From the analysis, it is clear that there are some reactions occurring. Some of these reactions occur in the 80-85 m range which is the location of one thermal source. The largest contributor would be methane oxidation because of its high concentrations and large energy release compared to the other reactions. However, it can be concluded that chemical reactions are not contributing significantly to the thermal bump.

5.2. Solar radiation

Despite its high latitude, significant amounts of solar radiation reach the surface of Antarctica. The incident angle at these high latitudes is rather high. In some ways the radiation in the region is even more intense than other areas because of the higher portion of ultraviolet wave length reaching the surface as a result of the ozone hole. Another consideration of solar radiation in Antarctica is the unusual cycles. In the winter months, Antarctica experiences months of darkness but in the summer, there is a several month long period with constant day light. This odd pattern arises from the earth's inclination and the orbit of earth around the sun. The sun emits an electromagnetic spectrum according to Plank's law at a temperature of about 5777k. This spectrum profile peaks in the visible region but still contains significant energy in non-visible portions such as infrared and ultraviolet as seen in figure 22. The sun produces a total of 1365 W/m2 at earth's orbital distance (NASA,2015). As the radiation passes through the earth's atmosphere, some wavelengths are effectively blocked. This is particularly true of the ultraviolet wavelengths and to a lesser degree in some infrared wavelengths as seen in figure 23.

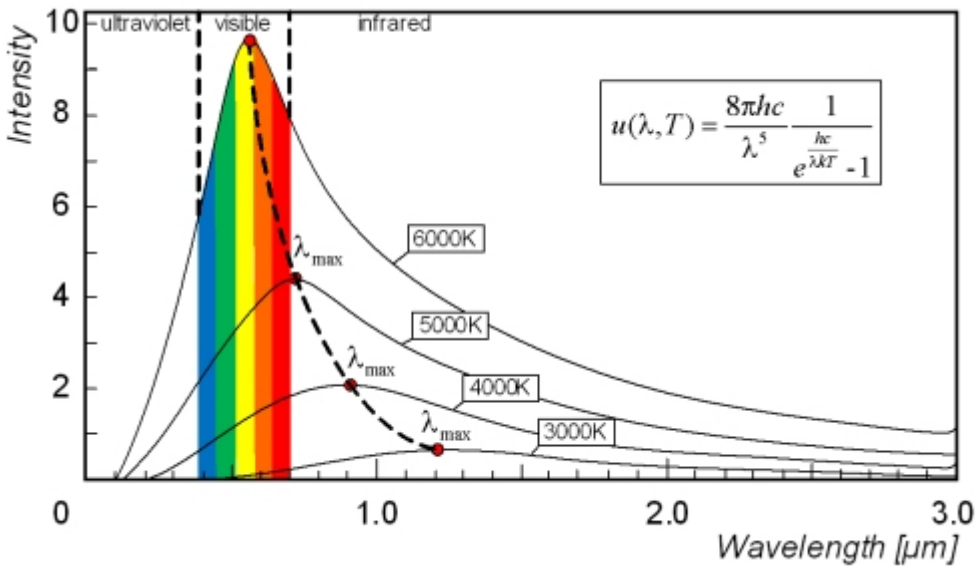

Figure 22. Plank distributions of black body electromagnetic radiation. The sun is approximately 5777K producing a profile that peaks in the visible range (NASA, 2015). Image credit: Vratislav Michal

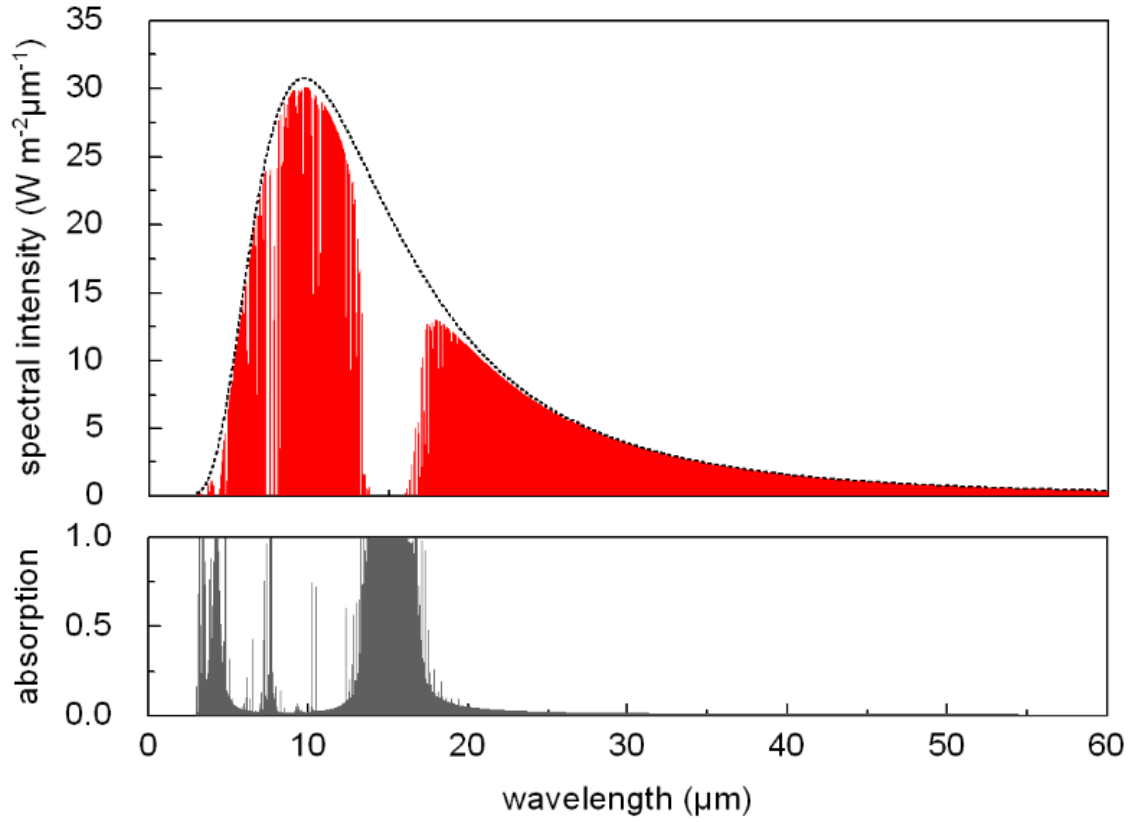

Figure 23. Atmospheric absorption of solar radiation and resulting radiation spectrum after passing through the atmosphere. Ultraviolet wavelengths and to a lesser degree in some infrared wavelengths are particularly effected. Image credit: Haseler

Prior to reaching the lake, however, the light must first pass though the ice. Lake Untersee has an ice layer ranging from 2.2-3.8 m with an average thickness of 3 m (Wand et al., 1997). McKay et al., 1994 investigated the transmissivity of Antarctic lake ice. They determined the transmissivity to be about 5% for the range of 400-700nm. This value accounts for bubbles and particles such as sand in the ice. Andersen et al. 2011 measured an average transmissivity of 4.9% +/- 0.9% for wavelengths between 400-700nm at 12 locations on Lake Untersee ice. Ice is known to absorb infrared wavelengths effectively. Thus the solar radiation passing through the ice will have only negligible energy contribution in the inferred range. The annual average solar radiation reaching the surface of Lake Untersee is 99.2 W/m2 (Andersen et al., 2015). This value was determined by measuring the solar radiation across a 4 year period and is very similar to values of other locations in Antarctica. In Lake Untersee Andersen et al. 2011 showed that radiation is reaching depths of 100m in the large basin in enough quantity to support photosynthetic life.

The range of 400-700nm is an important range of the electromagnetic spectrum because it is the wavelengths used by photosynthetic organisms. This range is known as PAR for photosynthetically active radiation. Chlorophyll is a biomolecule responsible for harvesting light in the photosynthetic pathway. Though there are several types of Chlorophyll, Chlorophyll a and Chlorophyll b are among the more important and more studied. Figure 24 depicts the absorbance spectra for chlorophyll a and chlorophyll which both contains 2 primary peaks. The largest peak is around 430nm while the smaller peak is around 640 for Chlorophyll a. Because of the importance of primary producers and photosynthetic organisms for an ecosystem, PAR is a frequently studied portion of the electromagnetic spectrum. PAR lends itself to study also because it spans the majority of the visible range where most of the solar energy occurs.

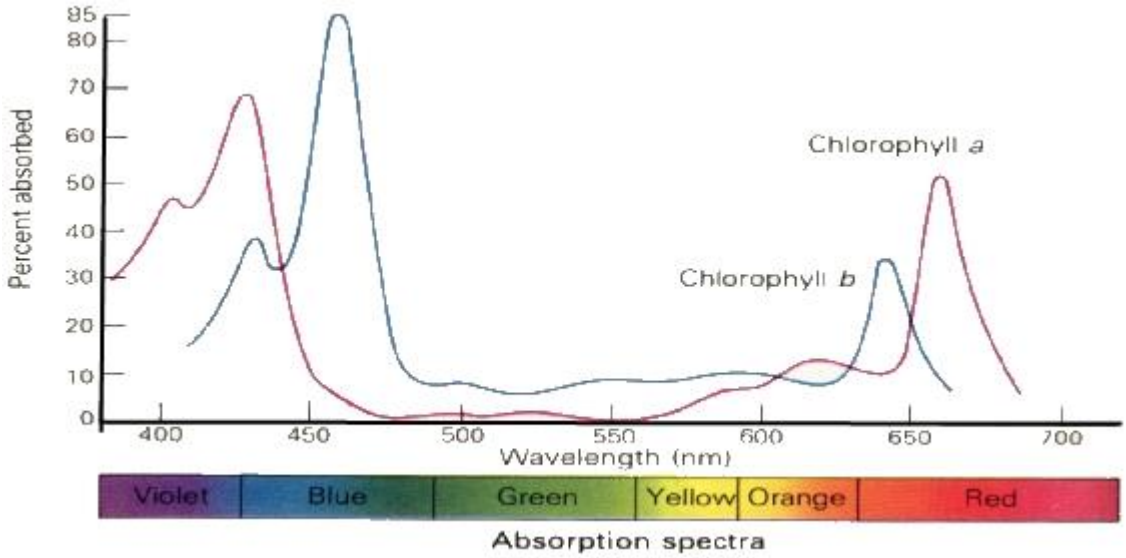

Figure 24. Spectral absorbance profile for Chlorophyll a and Chlorophyll b. Chlorophyll a and Chlorophyll b are the dominant proteins responsible for light harvesting in photosynthesis. Their active ranges span 400 to 700nm which is the boundaries for PAR. Image credit: Austin Community College District

Radiation in the PAR range was measured using a LI-193 spherical quantum sensor which was lowered through a hole drilled in the ice (LI-Core). The hole was subsequently filled to prevent error from light not passing through the ice. Measurements were recorded at 5m increments until 75 m where 1 m increments were used. To normalize the measurements in the water column for changing surface conditions, surface radiation was measured simultaneously using a LI-190 cosine corrected sensor (LI-Core).

For this analysis, the profile was scaled such that the radiation energy at 0m was 2.5 W/m2. 2.5 W/m2 comes from an assumption of 100 W/m2 mean annual radiation, 5% transmissivity, and 50% of the spectrum occurring in the PAR range (McKay et al., 1994; McKay personal communication, 2015). Thus, 100 W/m2 * 0.05 * 0.5 = 2.5 W/m2 at 0m. The resulting profile is shown in figure 25. Despite the clarity of the upper portion of the water column, significant portions of light are removed. The coefficient of diffuse attenuation is 0.034 m-1 and attenuation is very stable in the upper water column as seen in figure 26. This value is similar to other Antarctic lakes (Vincent et al., 1998).

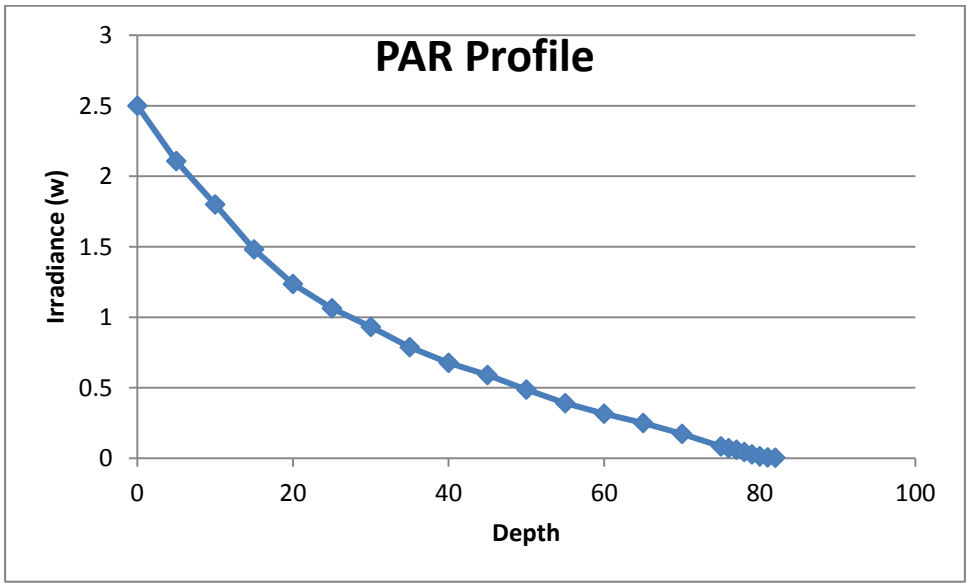

Figure 25. PAR radiation profile. Despite the clear water, much of the light is absorbed in the upper water column.

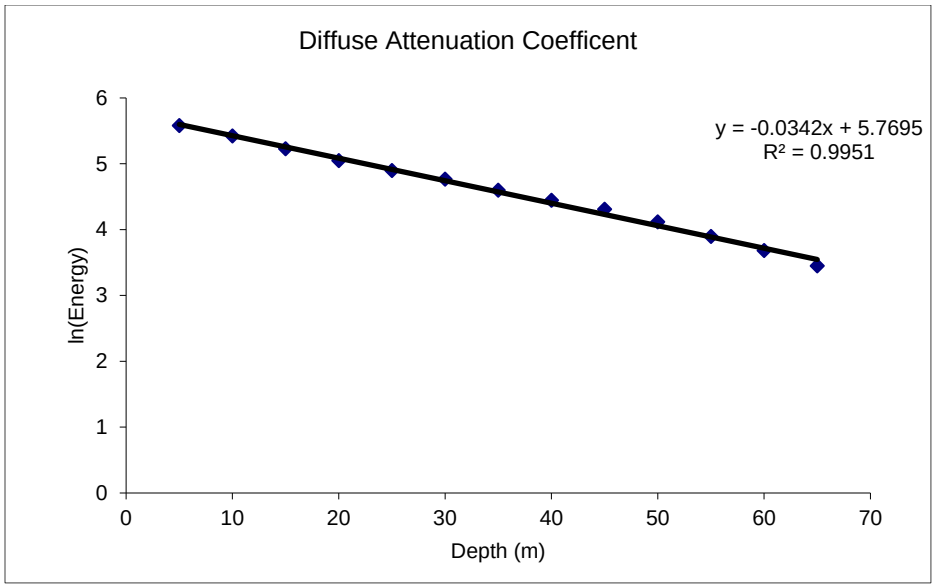

Figure 26. Estimate of the diffuse attenuation coefficient.

To estimate the amount of heat produced, it was assumed that all light not passing through to the next depth was converted to heat. The accuracy of this assumption should hold under most circumstances. Exception would include radiation induced reactions i.e. photoreactions, and photosynthesis. Photosynthesis, though it converts radiation energy to chemical bonds, is very inefficient. C3 photosynthesis is 4.6% efficient while C4 photosynthesis is 6% efficient at current atmospheric conditions (Zhu et al., 2008). Thus, even if there is a photosynthetic component, it should only introduce a 6% error at most. The amount of energy reaching the thermal bump portion of the water column at 65 m is 0.250 W/m2. This is 156% of the required source. However, the required heat source value of 0.16 W/m2 was arrived at by averaging values from two years which differed significantly. One of these years, the value was 0.203 W/m2 which is within 20% of the incoming energy.

The energy generation function then is just the derivative of the PAR profile. A forward approximation was used to estimate the derivative numerically. Values were then shifted to represent the center between nodes. This was done to offset the effective shifting from applying the forward method. The result is shown in figure 27. The shape of the curve is significant because it has two peaks. The first peak occurs at 72.5 m and the second occurs at 78.5 m. These locations are very similar to the 71.3 and 80.6 m locations determined by the thermal analysis.

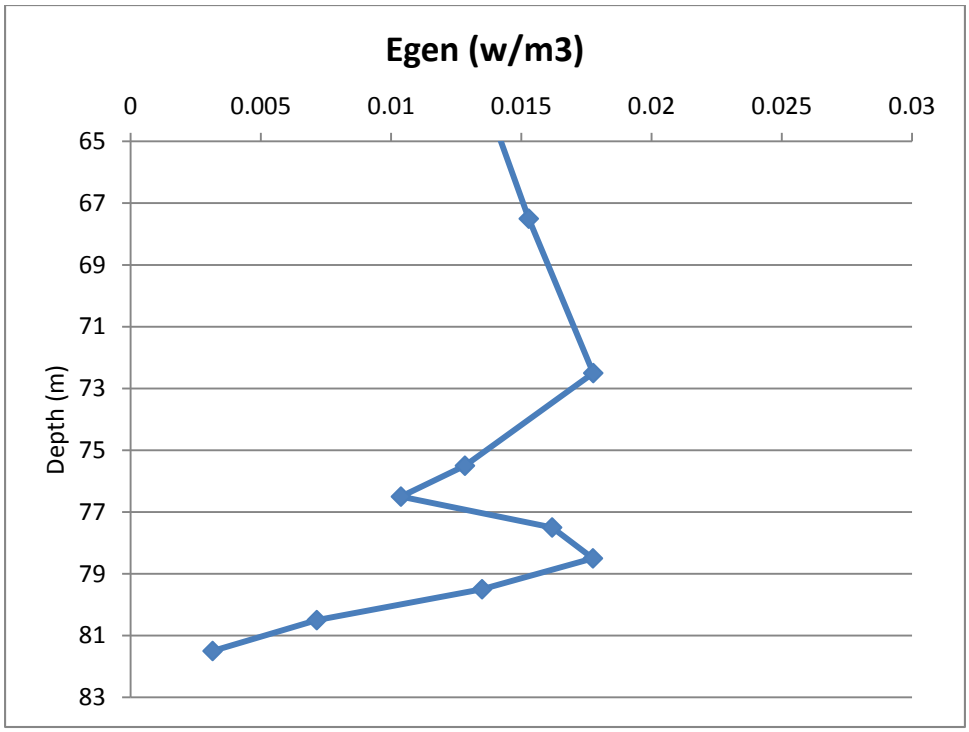

Figure 27. Energy generation function approximated from the PAR profile.

There are clearly sources of opacity in the water column that are attenuating light. The top source has more radiative energy to capture and is less opaque while the lower source has less available energy but is more opaque. The diffusive attenuation coefficients in the lower water column confirm this as seen in figure 28. The physical sources for the opacity are likely microbes in the water column. The case for the upper source is quite strong. Figure 29 is a profile of Chlorophyll a. The profile has 2 sharp peaks in the range from 70-75 m indicating the presence of photosynthetic organisms. As discussed above, these organisms are capable of converting only 4-6% of the radiative energy into chemical bonds leaving the remaining portion for heat. At depths below 85 m there is a gradual increase in measured Chlorophyll a. This is likely not a response from organisms but an interference from the dissolved organic carbon known to be present in these depths (table 5). From the chemical analysis, there were several reactions identified around 80 m. While these reactions themselves were not enough to produce the thermal bump, they are likely supporting microbial life. These microbes then act as a source of opacity that converts radiation into thermal energy.

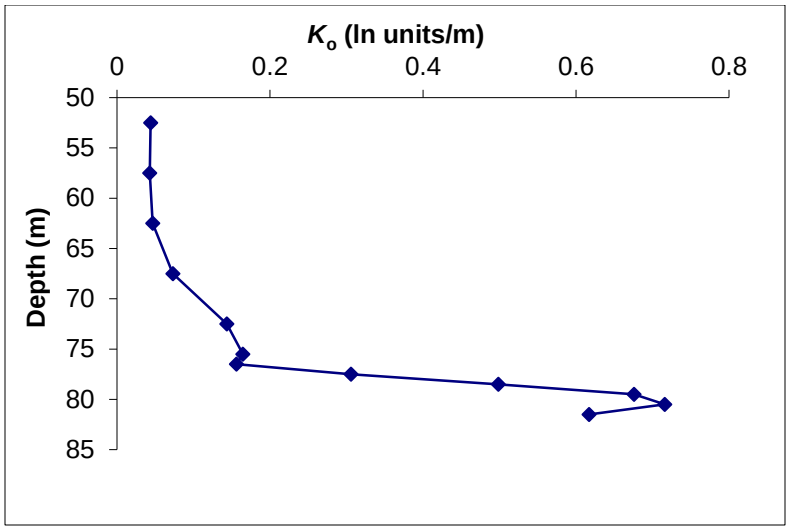

Figure 28. Diffusive attenuation coefficients in the lower water column. Between 70 and 75 m there is a slight increase in Ko and a lager increase at 80m.

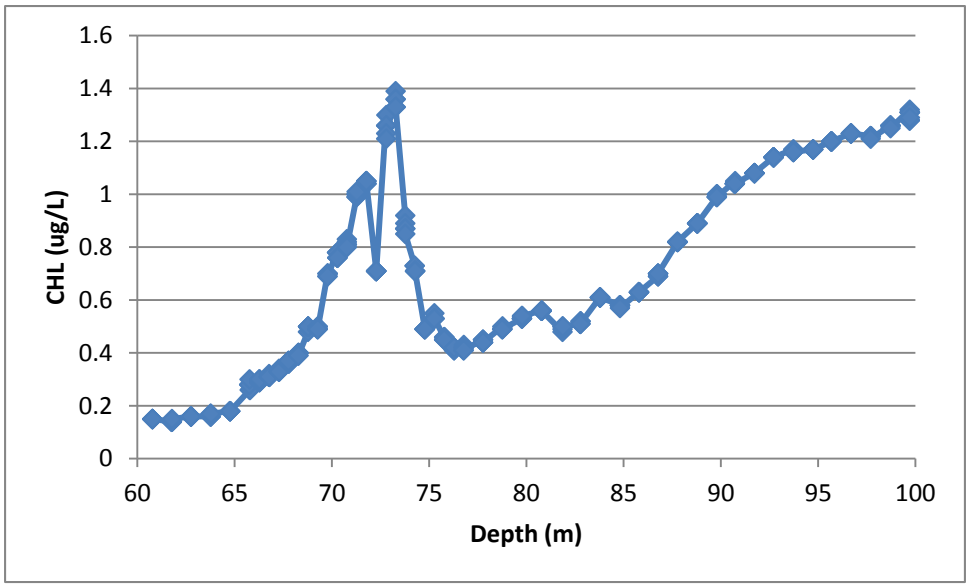

Figure 29. Chlorophyll a profile. There are two peaks between 70 and 75 m which indicate the presence of photosynthetic microbes. The increase at depths below 80 m is likely a result of interference from the dissolved carbon in these depths of the water column.

6. Stability

The thermal analysis and search for energy sources were all based on the assumption of diffusion dominated regime i.e. no convective water flows.

The UNESCO formula was used to convert conductivity to “salinity” which is frequently interpreted as TDS (Spigel and Priscu, 1996; Lewis, 1980; Millero and Poisson, 1982; Millero et al., 1980; Fofonoff and Millard, 1983). The density for each depth was calculated using the TDS calculation and measured temperature. Stability of the water column was evaluated using the UNESCO formula and calculating the

slope of the density profile. The error bars associated with the density estimates were determined by adding/subtracting the published measurement accuracy of the sensor to the measured values which is assumed to be the maximum possible deviation from the measured value (YSI, 2015). Calculations were carried out on these deviated values to determine the effects of measurement error on density estimates. The error of the UNESCO model was not considered in determining the error.

The existence of a thermal pocket is an interesting prospect because it should be expected that the warmer water would create an instability and result in a convective mixing which is contrary to the assumption of a fully diffusive regime made by analysis above. Temperature, however, is not acting alone but the presence of TDS must be considered as well. For all depths in the anoxic hole (below 50 m) except 65 m, density increases with depth as seen in figure 30. Despite the increase in temperature of the bump and subsequent decrease below 4C, the density maximum of water, the column remains stable because of increasing TDS with depth as shown in figure 31. In fact, the TDS concentration is such that the bump could be heated to approximately 8C before becoming unstable. The impact and reality of the slight instability at 65 m is not clear as the estimate is well inside the error bars of the measurements.

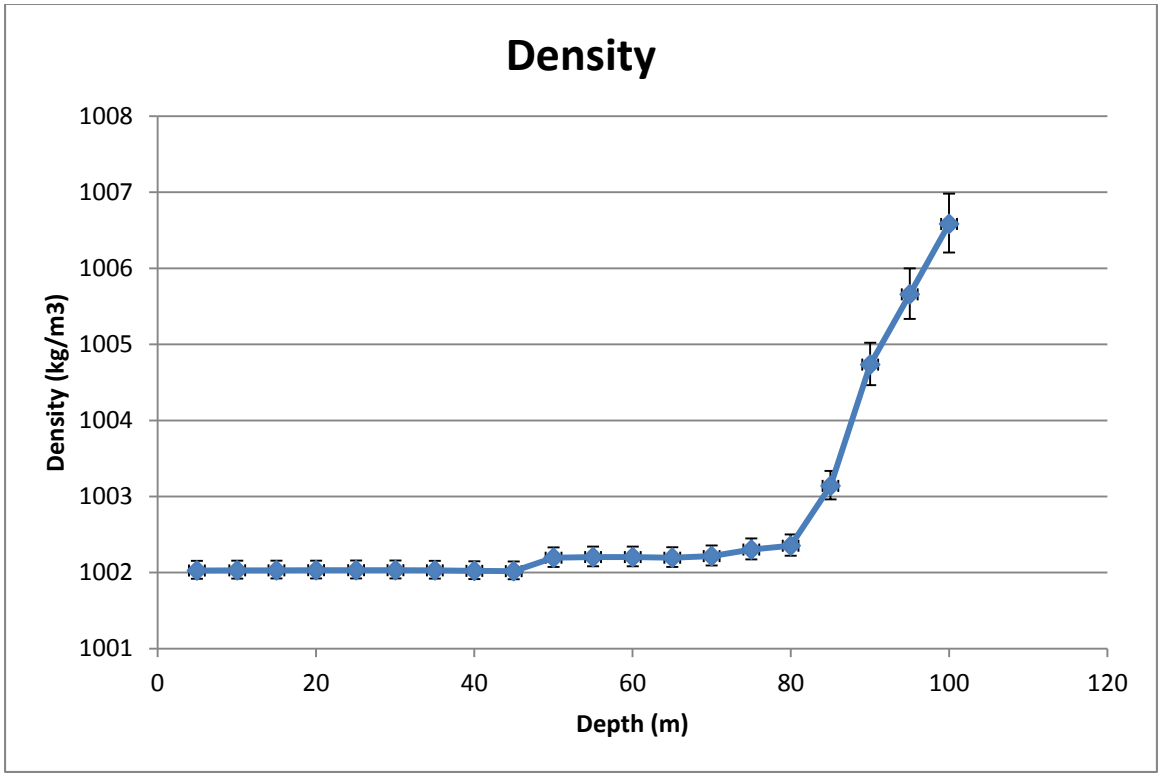

Figure 30. Density profile of the anoxic hole. In the diffusive region density increases with depth except possibly at 65 m.

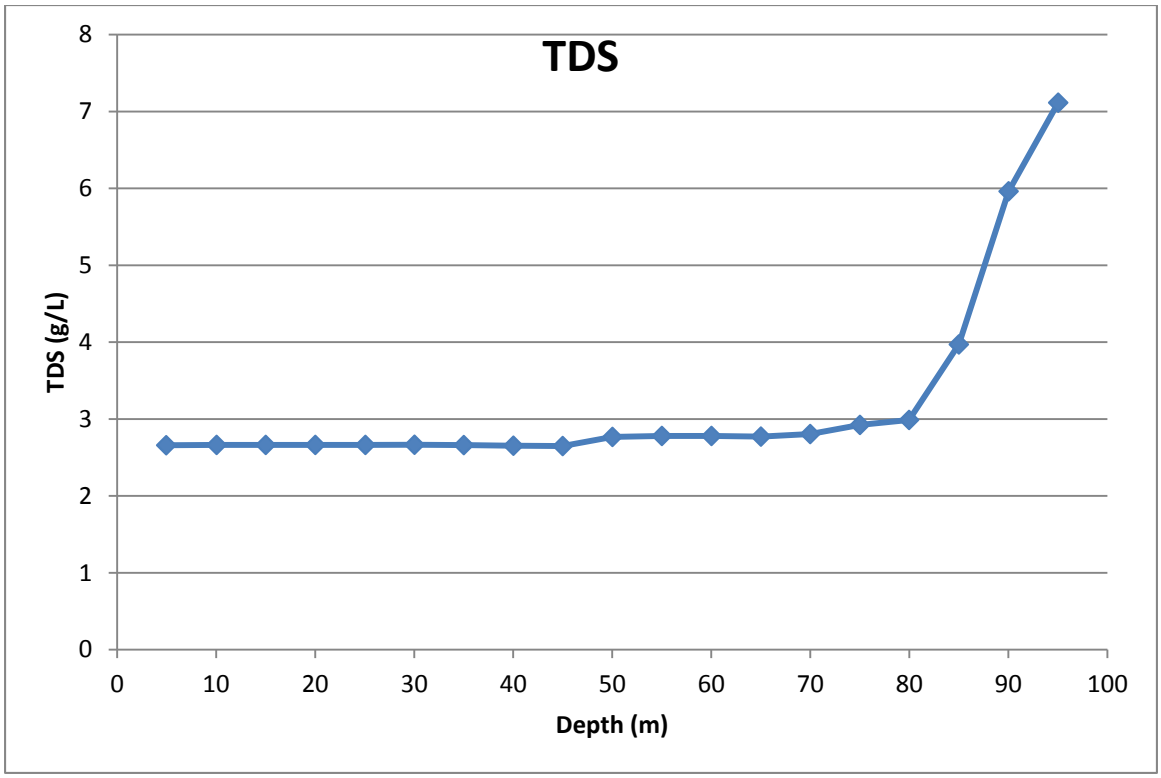

Figure 31. Total dissolved solids profile. The profile is very similar to the density profile suggesting that TDS dominates the density of the water over the thermal changes.

7. Field work

The field work described in this section is not directly connected to the project undertaken during the internship period. However, it is related to the larger aim of identifying biomarkers and unraveling the mechanisms used by life in extreme environments. The first field excursion was undertaken with the aim of studying snow algae. The second was directed at studying desert microbes.

7.1. Snow Algae

Snow algae are an understudied model organism. Unlike Antarctic and desert organisms, the interesting aspect of snow algae is not the extreme environment in which they live. Snow is colder than many environments but not cold enough to require special coping mechanisms. The current model for snow algae is that each of the basic requirements for the organism are put in place at a some mostly independent time. However, it's not until all of the needs are met that growth can occur. Once all of the pieces are in place, growth can be quite rapid. One reason that this is the case for snow algae is that the snow is placed fresh every year. Snow by itself has no nutrients nor algae in place when it falls. Thus, nutrients and algae must be transported in. In addition, lighting conditions must melt some of the snow to make accessible water and provide energy for photosynthesis.

This is an interesting model for astrobiology because it is possible to separate the processes that set each parameter and illustrates how and to what extent each parameter influences the growth. Potentially on other worlds, all of the parameters are met but if there is no source of life then nothing

will grow. Finding all of the required parameters without active growth would suggest that there is no life present. This is an important and rare piece of evidence because it is confirmatory of the null hypothesis.

7.2. Mojave Desert

Deserts are good analogs for Mars because of the dry conditions. Understanding the mechanisms that microbes employ to cope with low water availability is informative to potential life forms on Mars. One mechanism is employed by a community known as crust. Crust consists of small, multi-organismal communities frequently including Linchen and Cyanobacteria which form on the desert surface. However, the formation process is largely unknown. The McKay group operates several weather stations and maintains several study sites in the Mojave aimed at studying crust formation and other desert processes. Specific locations include Badwater in Death Valley and Ubehebe Crater.

8. Benefits to the student of the internship

This internship experience has been very beneficial to my career both in the near term and longer outlook. Experience is something that doesn't have an expiration. This is particularly true of problem solving approaches. Working with Dr. McKay has been an excellent opportunity to hone my problem solving skills. This has been accomplished through witnessing Dr. McKay's approach to problems and research questions as an outside view point. For example, when other students present their work at our weekly group meeting, seeing the questions that he asks and his thoughts about the results is very informative about his thought process and approach. A second avenue for learning Dr. McKay's approach to problem solving is more internal. While working on my project I was frequently confronted with problems. When these problems arose I would do my best to solve them with my approach to problem solving. Often this would be successful but sometimes it wasn't. In the cases where I had reached a "dead end" Dr. McKay often found solutions thereby illustrating a new approach. Because of my familiarity with the project and own attempts at problem solving, his solutions provided an opportunity to measure, gauge, and improve my problem solving ability. This process was like practice for problem solving and I have added many new tools to my metaphorical problem solving tool bag.

Another benefit from my internship at NASA is the new contacts that I have made. Some of these contacts are useful at the current time while others may become useful in the future. Examples of contacts that may be come valuable in a longer time frame include the other interns working at NASA. In particular, an undergraduate from Canada, undergraduate from France, and undergraduate from California all have aspirations to work in the Aerospace industry and thus may become collogues. In the shorter time frame, the relationships I have built with Dr. McKay and some of his collaborators, Dr. Dale Andersen and Dr. Alfonso Davila, will likely prove valuable as I undertake my PhD in the same research field. These researchers could give input on my PhD project, or become future post doc advisors or collaborators. Additionally, Dr. McKay has a current proposal under review for a Discovery class mission to Mars which could turn into a job opportunity prior to starting my PhD or after my PhD is complete. In the current time frame, a letter of recommendation from Dr. McKay for PhD and funding applications is valuable.

A final benefit from this internship is an expected publication to be submitted to the journal Antarctic Science. This publication will aid in future endeavors in the field of research and solidify my connection to NASA and Dr. McKay, a world renowned astrobiologist, in the scientific literature.

9. Conclusion

The search for life is one of the most compelling scientific endeavors underway and one that could be successful within the current century. Life is currently undefinable which both makes the search for other life difficult but proves the need for the search. Without other examples, understanding the far-reaching implications of biological functions is hindered. As there are no other examples, the best focus is studying life as it is found on earth. Extreme environments such as hydrothermal vents, deserts, and Antarctic lakes can provide clues of what to search for on other worlds.

One analog for icy moons of Saturn and Jupiter is Lake Untersee. Lake Untersee has an interesting thermal anomaly in the form of an unexpected layer of higher temperature water. A thermal analysis of the bump revealed two sources are needed to explain the observed profile. The physical explanation of these sources is hypothesized to be light attenuated by the presence of microbes at the depths where the thermal sources are located. This hypothesis is supported by the photosynthetically active radiation attenuation profile which has two peaks at similar depths to the thermal sources, and the similar magnitude of energy between the incoming radiation and heat required to maintain the thermal profile. Evidence for microbial presence at these two depths includes a peak in chlorophyll at the same depth as the upper source and active chemical reactions in the region of the lower peak including maximum rates of at least two potentially life supporting reactions.

Recommendations for future work include:

1. Sample the temperature profile with higher resolution at depths near the thermocline
2. Confirm presence of microbial life using small subunit ribosomal RNA techniques
3. Measure the cell density in the water column and predict the opacity of the water as a function of cell density.

Other activities during the internship included two field trips to Mount Lassen and the Mojave Desert. In addition to these trips, the student benefited from the internship experience in other ways. These benefits include contacts and networking, honing problem solving skills, access to a world renowned astrobiologist, and an expected publication.

References

Andersen, D., D. Sumner, I. Hawes, J. Webster-Brown and C. McKay. 2011. Discovery of large conical stromatolites in Lake Untersee, Antarctica. Geobiology. 9: 280-293.

Andersen, D., C. McKay, and V. 2015. Climate conditions at perennially ice-covered Lake Untersee, East Antarctica. Journal of Applied Meteorology and Climatology. 54: 1393-1412.

August, G. et al. 1999. The effects of peanut butter on the rotation of the earth. Abrahams, M. eds. Translator. August, G. Annals of Improbable Research. Switzerland.

Austin Community College District. “PreLab 7.4” BIOL 1406. Austin Community College District. Accessed 31 July 2015. < http://www.austincc.edu/biocr/1406/labm/ex7/prelab_7_4.htm >

CRC. 1976. Handbook of Chemestry and Physics, 57th ed. CRC Press, Boca Raton FL.

Earle, R. 1983. Unit operations in food processing second edition. Pergamon Press. Oxford, UK.

Fofonoff, N. and R. Millard. 1983. Algorithms for computation of fundamental properties of seawater. Unesco technical papers in marine science 44. Division of Marine Sciences, Unesco, Paris. 53pp.

Haseler,. M. “What does CO2 really Contribute to global warming – 2nd Update” Scottish Sceptic. Accessed 31 July 2015. < http://scottishsceptic.co.uk/2011/03/17/what-does-co2-really-contribute-to-global-warming-2nd-update/ >

Lewis, E.. 1980. Practical Salinity Scale 1978 and its antecedents. IEEE Journal of Oceanic Engineering 1 OE(5): 3-8.

LI-COR. 2015. Principles of Radiation Measurement. LI-COR.

McKay, C., G. Clow, D. Andersen and R. Wharton. Light transmission and reflection in perennially ice-covered Lake Hoare, Antarctica. Journal of Geophysical Research. 99(C10): 20,427-20,444.

Millero, F., C.-T. Chen. A Brandshaw, and K. Schleicher. 1980. A new high pressure equation of state for seawater. Deep-Sea Research. 27(A): 255-264.

Millero, F. and A. Poisson. 1981. International one-atmosphere equation of state of seawater. Deep-Sea Research. 28(A): 625-629.

Milo et al. Nucl. Acids Res. (2010) 38: D750-D753. From BioNumbers 6 digit ID, e.g. "BNID 100986, Milo et al 2010".

NASA. “Sun” Solar System Exploration. NASA. Accessed 31 July 2015. <http://solarsystem.nasa.gov/planets/profile.cfm?Display=Facts&Object=Sun >

Reesburgh, W. 2007. Oceanic Methane Biogeochemistry. Chemistry Review. 107: 486-513.

Simon Fraser University. “Alternative Definitions of Life: Perspective Matters” President’s Dream Colloquium. Simon Fraser University. Accessed 31 July 2015. <https://www.sfu.ca/colloquium/PDC_Top/OoL/whatislife/Vikingmission.html >

Steel, H., C. McKay, and D. Andersen. 2015. Modeling circulation and seasonal fluctuations in perennially ice-covered and ice-walled Lake Untersee, Antarctica. Limnology and Oceanography. 00: 1-17.

Tate, K. 2013. “Occupy Mars: History of Robotic Red Planet Missions (Infographic)” Space.com. Accessed 31 July 2015. < http://www.space.com/16575-mars-exploration-robot-red-planet-missions-infographic.html >

Vincent, W., R. Rae, I. Laurion, C. Howard-Williams and J. Priscu. 1998. Transparency of Antarctic ice-covered lakes to solar UV radiation. Limnology and Oceanography 43(4): 618-624.

Vratislav, M. 2009. Design of CMOS analog integrated circuits as readout electronics for High-TC superconductor and semiconductor terahertz bolometric sensors. University Pierre et Marie Curie PhD Thesis.

Wand, U., G. Schwarz, E. Bruggemann and K. Brauer. 1997. Evidence for physical and chemical stratification in Lake Untersee (central Dronning Maud Land, East Antarctica. Antarctic Science. 9(1): 43-45.

Wand, U., V. Samarkin, H.-M. Nitzsche and H.-W. Hubberten. 2006. Biogeochemistry of methane in the permanently ice-covered Lake Untersee, central Dronning Maud Land, East Antarctica. Limnology and Oceanography 51(2): 1180-1194.

YSI incorporated. 2015. Environmental monitoring systems manual. YSI incorporated.

Zhu, Xin-Guang, S. Long, and D. Ort. 2008. What is the maximum efficiency with which photosynthesis can convert solar energy into biomass?. Current Opinion in Biotechnology. 19(2): 153-159.